Technical specifications of the system of geophysical sensors

FP7 – DIGISOIL Project Deliverable D1.1

N° FP7-DIGISOIL-D1.1
March 2009
Revision 1

DIGISOIL

Geoscience for a sustainable Earth
brgm

Technical specifications of the system of geophysical sensors

FP7 – DIGISOIL Project Deliverable 1.1

N° FP7-DIGISOIL-D1.1
March 2009
Revision 1

S.Lambot (UCL/FZJ)
With the collaboration of
G.Grandjean, K.Samyn (BRGM), I.Cousin, J.Thiesson (INRA), A.Stevens (UCL), L.Chiarantini (GAV), T.Dahlin (ABEM)

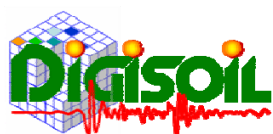| Checked by:	Approved by:
Name: S.Lambot	Name: G.Grandjean
Date:15/01/09	Date: 26/01/09
☑	☑

BRGM's quality management system is certified ISO 9001:2000 by AFAQ.

Geoscience for a sustainable Earth
brgm

Synopsis

The present deliverable concerns the first task of the DIGISOIL's WP1. Requirements of the proposed system according to the data acquisition and management points of view are first studied. These requirements lead to organise the different components of the system in the frame of a functional analysis where objectives, products and functions are clearly presented.

Then, a state of the art on the different geophysical sensing techniques able to contribute to the DIGISOIL's objectives is performed. Each technique is reviewed in terms of measurement principles, processing and applications, strengths and limitations, and availability of commercial and non-commercial sensors. This part leads to identify the techniques being in the scope of the projects from those considered not suitable enough.

Finally, for all of these techniques, a study of possible technical solutions is conducted for identifying the best active source, sensors, measuring strategy and equipment. A synthetic table is finally proposed to roughly identify the composition of the integrated system that will be tested in the next field experiments.

Contents

List of illustrations

List of tables

1. Introduction

1.1. DIGISOIL'S CORE OBJECTIVES

The multidisciplinary DIGISOIL consortium intends to **integrate and improve *in situ* and proximal measurement technologies for the assessment of soil properties and soil degradation indicators, going from the sensing technologies to their integration and their application in (digital) soil mapping (DSM)**. In addition, our SMEs experience will allow taking **into account the feasibility of such developments based on economical constraints, reliability of the results and needs of the DSM community**.

In order to assess and prevent soil degradation and to benefit from the different ecological, economical and historical functions of the soil in a sustainable way, there is an obvious need for high resolution and accurate maps of soil properties. The core objective of the project is to explore and exploit new capabilities of advanced geophysical technologies for answering this societal demand. To this aim, DIGISOIL addresses four issues covering technological, soil science and economic aspects (Figure 1): (i) the validation of geophysical (in situ, proximal and airborne) technologies and integrated pedo-geophysical inversion techniques (mechanistic data fusion) (ii) the relation between the geophysical parameters and the soil properties, (iii) the integration of the derived soil properties for mapping soil functions and soil threats, (iv) the evaluation, standardisation and sub-industrialization of the proposed methodologies, including technical and economical studies.

With respect to these issues, the milestones of the DIGISOIL project are:

1. To develop, test and validate the most relevant geophysical technologies for mapping soil properties: **geoelectric, seismic, GPR/EMI, magnetic and airborne hyperspectral**;

2. To establish correlations between the measured geophysical measurements and the soil properties involved in soil functions / threats (**erosion, compaction, organic matter decline, salinisation and shallow landslides**) by using innovative data processing (inversion) and correlation protocols;

3. To evaluate the societal impact of the developed techniques by investigating their relevance relative to the end-user needs, the technical feasibility and the cost effectiveness;

4. To produce an exploitation plan including the standardization of the processes and the technical specifications of the developed methodologies describing the system components in terms of equipment (sensors, acquisition system, mobile vector), techniques (signal processing, inversion or fusion processes, specialization) and operational protocols.
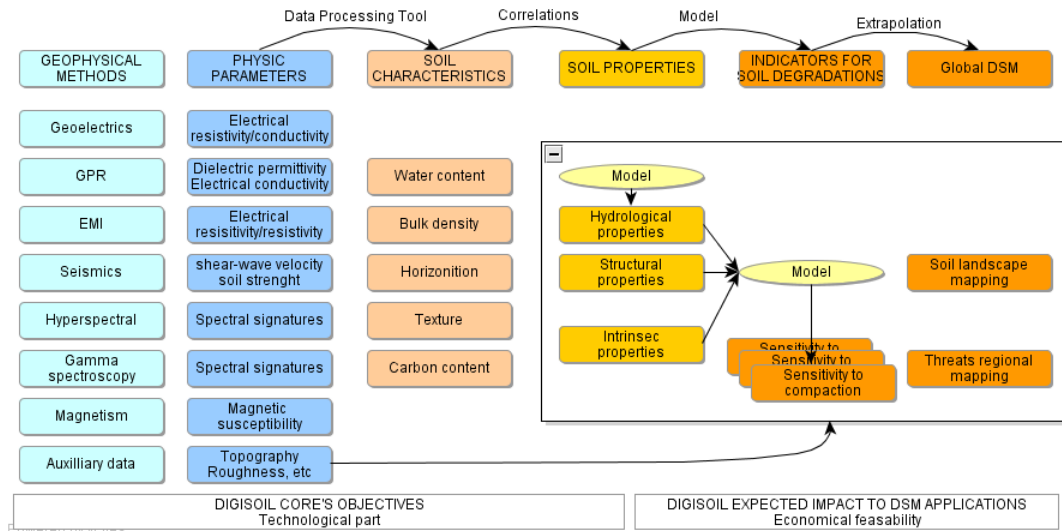
Figure 1: Digisoil's concept.

1.2. REQUIREMENTS REQUESTED BY DIGISOIL

DIGISOIL requires a strong collaboration between geophysicists, soil scientists and industrial partners for developing a new soil mapping product featured by at least the following characteristics:

- Integrated and efficient technological tools for mapping soil properties from the field up to the catchment scale.

- Innovative quasi-continuous seismic methods adapted for mapping soil properties involved in soil threats and soil functions (compaction, erosion, biomass, production …).

- Highly sensitive/wideband GPR and EMI technologies with full-waveform analyses;

- Ultra Light Motorised hyperspectral flying sensor campaigns to characterise topsoil organic matter content (and therewith avoiding the use of costly classic airborne campaigns).

To identify more precisely what could be the needs of DIGISOIL, a functional analysis was performed. This study aims to identify what are the hierarchical products the project has to deliver and what are their related constraints and interdependencies. Figure 2 shows the diagram of such analysis. Il the following sections, we will focus our attention on what is necessary to produce geophysical parameters maps and what are the constraints related to them.

1.2.1. In terms of measuring methods

In the last decades, geophysical prospecting applied to the subsurface characterization has been of an increasing interest, particularly in Soil Science. Major advances in this technological domain can be attributed to the development of integrated measure systems, increasing computing power, equipment portability and hardware/software diffusion. In this context, two kinds of technological platforms can be involved: ground-based and proximal technologies, respectively working from the surface and from a ligh airborne vector.

Ground-based geophysical instruments are now equipped with digital signal processing and recording capabilities previously restricted to large corporate computing centres. This improved computational capacity has provided investigators with near real-time results that, in turn, drive improvements in instrument sensors and processing algorithms. Identically, recent airborne geophysics sparked off a strong interest due to the possibilities of flights with civil airplanes equipped with optical, thermal or hyperspectral sensors. The most common methods which took advantages of these enhancements and the related parameters are listed in Table 1.

Geophysical methods	Physical parameters
Ground-penetrating radar (GPR):	Dielectric permittivity, electric conductivity, magnetic permeability, frequency dependence of these electromagnetic properties
Seismic reflection and refraction:	Volume and shear-wave velocities
Electromagnetic induction (EMI):	Electrical resistivity (electric conductivity and frequency dependence)
Electrical resistivity (geoelectric):	Electrical resistivity (almost zero-frequency)
Gravity:	*Density*
Magnetics:	Magnetic susceptibility and viscosity
Airborne thermic:	*Surface temperature*
Airborne hyperspectral:	Spectral reflectance
Gammametry:	*Gamma spectrum (U, K, Th)*

Table 1: Main ground-based and airborne geophysical methods and related physical parameters. In italic, the methods that will not be integrated in the DIGISOIL's tool.

The purpose of the DIGISOIL project is to identify and bridge the technological gap to develop pertinent, reliable and cost-effective geophysical mapping solutions. Considering the new equipment and signal processing developments offered by recent scientific exploitations, the problem of carrying out soil data collections at the catchment scale using geophysical sensors can be foreseen in the near future, particularly for methods identified in the Table 1 (GPR, EMI, seismics, magnetics and airborne hyperspectral). Gravity and thermic methods will not be incorporated in DIGISOIL because of their low contribution to the characterization of soil properties related to above-cited degradation processes. For gammametry, several research actions have already been carried out to study the potential for soil properties

mapping. This technology has given satisfactory results and permits to map types of clay minerals in the topsoil through the analysis of U, K, Th anomalies in the gamma spectrum. We will not fully consider this method since it appears to be already used in the soil science community (Wilford and Minty, 2006). However, the information given by this technology being interesting in many aspects, we will integrate it as potential auxiliary data in our mapping strategy. This context is therefore favourable for the development of the DIGISOIL's mapping tools and products in relation to DSM applications.

1.2.2. In terms of the data acquisition system and data management

The DIGISOIL's specificities for the data acquisition system are strongly related to the production of geophysical parameters maps. The exigencies coming from such production can be summarized as follow:

- High speed recording: this condition is necessary to be able to produce a large quantity of data in order to cover the spatial domain of a map (1 to several parcels) with a relatively good resolution (5 to 15 m);

- Multisensor approach: this is the core of the methodology proposed in the project. The basics of this approach concern the possibility to recover soil parameters (density, water content, OM content, bedrock depth, etc) from a multiple interpretation coming from different measuring techniques. Knowing that a particular techniques won't be able to be efficient for all geological and pedological contexts, using several techniques optimize the chance to be successful for mapping a particular parameter;

- Experiments at the scale of parcels: the investigation dimensions is typically for producing detailed maps of physical parameters in order to estimate risk related to soils at the catchment's scale. Several hectares seems to be a reasonable surface dimension for observing large variations of soil parameters, characterizing local features, and being in the good range in terms of experiment costs, knowing that measurements are carried out from ground-based measuring systems;

- Spatial resolution of around tens of metres: from what is currently performed in precision agriculture or polluted soils mapping, the data acquisition systems are more or less able to deliver reliable measurements with a spatial precision less than 1 m. Taking into account the above cited constraints, a spatial sampling of around 10 to 50 m should be sufficient to cover the domains of investigations with a resolution in good agreement with phenomena needed to be observed.

- Resolution in depth: on the other hand, the needed resolution in the Z dimension should be able to describe the different pedological structures of the soils, and in particular i) the depth of the bedrock that is very important for modelling erosion processes and ii) the frontiers between horizons that are limits between domains of significant different soil properties.

These statements lead to propose a number of requirements for the DIGISOIL system within the WP1 and WP2 of the technical program. They concern respectively the data acquisition system and the data management strategy:

- The data acquisition system: the integration of selected sensors, the description of the PC-based unit controlling the data fluxes, some propositions for the vehicle that will move the system and a solution for the georeferencing protocol.

- The data management strategy: going from measurement to the soil properties is a difficult task where several aspects are necessary: (i) basic signal processing to enhance the signal to noise ratio, (ii) inversion techniques for retrieving geophysical parameters and finally (iii) fusion methods for increasing robustness of a specific parameter from a set of signals.
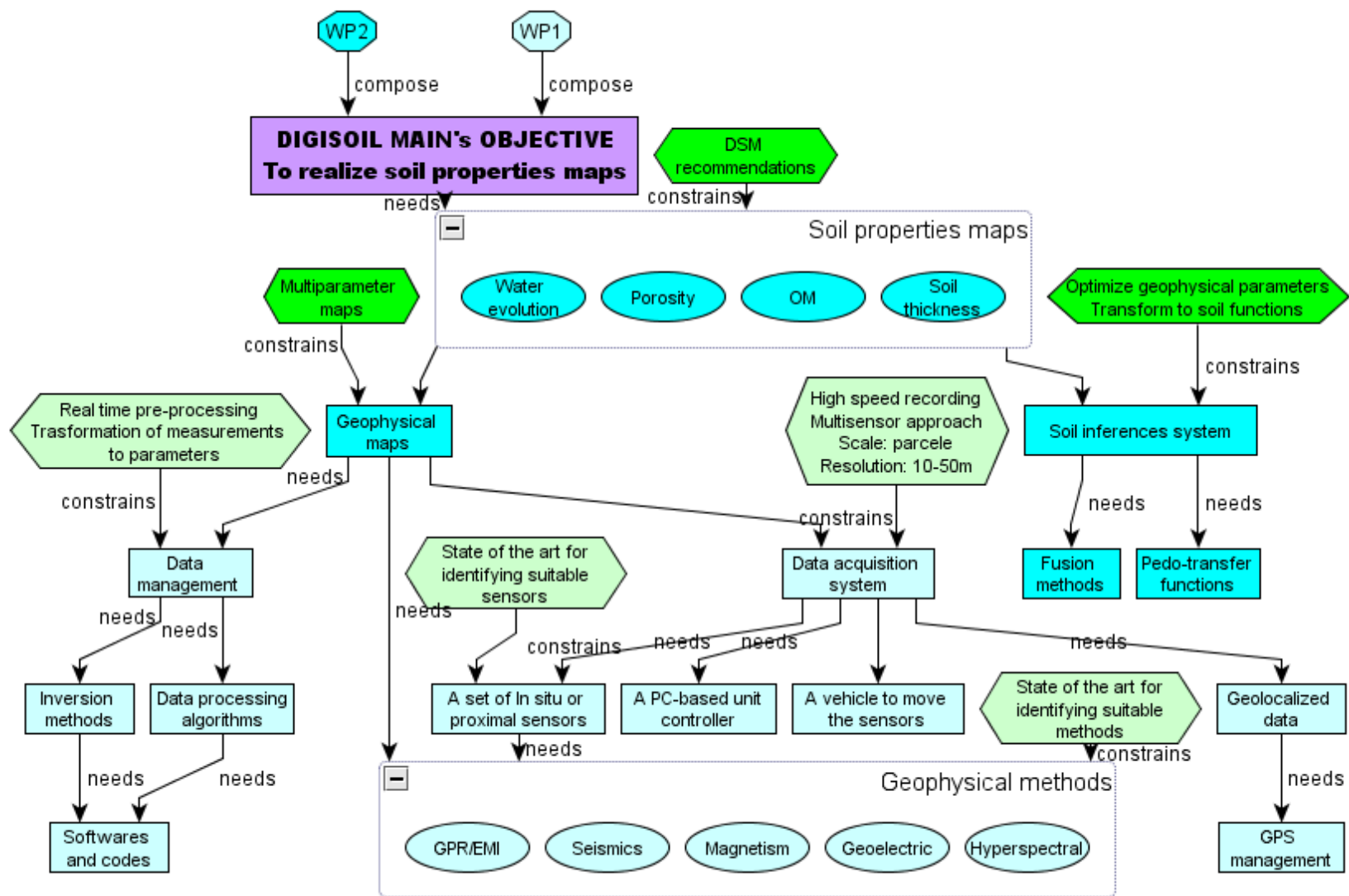
Figure 2 :Schematic functional analysis of the Digisoil's soil properties maps production

2. Review of geophysical sensors for soil characterization and imaging

2.1. INTRODUCTION

In the last decades, geophysical prospecting applied to the subsurface characterization has been of an increasing interest, particularly in Soil Science. Major advances in this technological domain can be attributed to the development of integrated measure systems, increasing computing power, equipment portability and hardware/software diffusion. In this context, two kinds of technological platforms can be involved: ground-based and proximal technologies, respectively working from the surface and from an airborne vector. Ground based geophysical instruments are now equipped with digital signal processing and recording capabilities previously restricted to large corporate computing centres. This improved computational capacity has provided investigators with near real-time results that, in turn, drive improvements in instrument sensors and processing algorithms. Identically, recent airborne geophysics sparked off strong interest due to the possibilities of flights with civil airplanes equipped with optical, thermal or hyperspectral sensors. The most common methods which took advantages of these enhancements are the ground-penetrating radar (GPR), seismic reflection and refraction, electromagnetic induction (EMI), electrical resistivity (geoelectric), gravity, magnetics, airborne thermic, airborne hyperspectral and gammametry.

The purpose of the DIGISOIL project is to identify and bridge the technological gap to develop pertinent, reliable and cost-effective geophysical mapping solutions. Considering the new equipment and signal processing developments offered by recent scientific exploitations, the problem of carrying out soil data collections at the catchment scale using geophysical sensors can be foreseen in the near future, particularly for the GPR, EMI, seismics, magnetics and airborne hyperspectral methods in which two categories are distinguishable: electromagnetic sensors and mechanical sensor (mechanical waves of seismic). Gravity and thermic methods will not be incorporated in DIGISOIL because of their low contribution to the characterization of soil properties related to degradation and threats. For gammametry, several research actions have already been carried out to study the potential for soil properties mapping, that's why the method will not be considered since it appears to be already used in the soil science community. However it will be integrated as potential auxiliary data in the mapping strategy if data are available on the Petite Beauce test site. This context is therefore favourable for the development of the DIGISOIL's mapping tools and products in relation to digital soil mapping (DSM) applications.

2.2. GEOELECTRIC

2.2.1. Measurement principles

The principle of the geoelectric method is based on an electrical resistivity survey which operates as follows: an electric current I is induced in the structure by means of contact electrodes (Ci electrodes) regularly arranged along a linear profile (Figure 3). This current invokes an electric field. Consequently, using other contact electrodes (Pi electrodes), the electric potential is measured in the neighbourhood of the actual path of electric streamlines. The current as well as the electric potential data are recorded and stored. Whenever there are inhomogeneities or changes in transmission of electric current beyond the surface, there will be a change of the electric streamline distribution. This causes an alteration of the electric potential distribution, which delivers information on the inhomogeneous state of the medium.
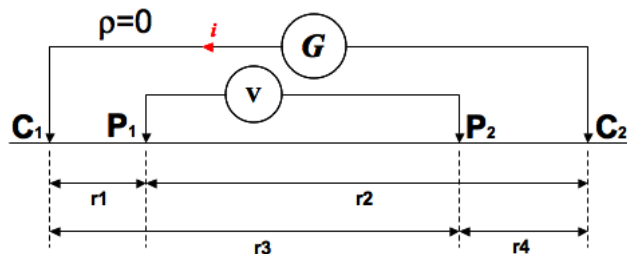
Figure 3 : Schematic geoelectrical quadripoles measurrments configuration

Different configurations of electrodes spacing for the measuring of electric potential and current exist, dealing with the number of Ci and Pi electrodes according to the objectives (commonly used quadripoles settings: Wenner-α/β, dipole-dipole and Schlumberger), and with r1, r2, r3 and r4 values, the distances between the electrodes. The depth of investigation increases with the dimensions of the device, but decreases with the resistivity of geological or soil layers. A conductive superficial layer is generally an inconvenience because it limits the depth of investigation and the resolution. Each 2D resistivity surveys configuration is associated with a range of electrodes spacing and sensitivity patterns (Figure 4).
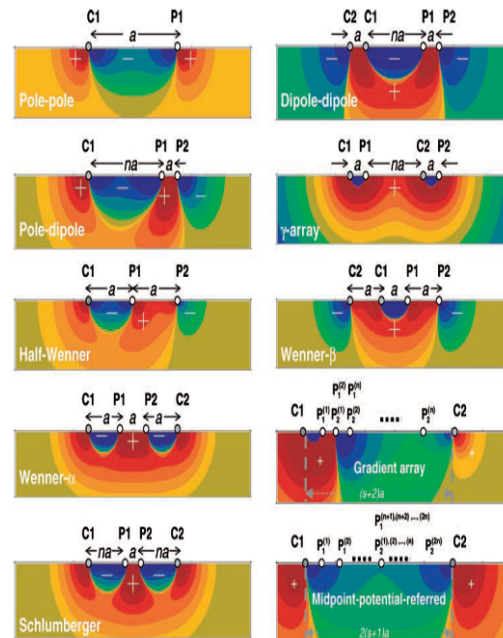
Figure 4: Diagrams of electrode arrays and their sensitivity patterns for 2D resistivity surveys (Torleif Dahlin et al., 2004)

2.2.2. State-of-the-art and applications

Widely developed for the characterisation of the unsaturated zone, measurements of the electrical resistivity have recently been applied to characterize soils (Banton et al., 1997). It simply consists in recording the difference in electrical potential in the soil when a (quasi-continuous) current is injected with electrodes devices described above. Profiles are then interpreted by inversion of visible resistivity using software like RES2DINV (Loke et al., 1996). At this stage of treatment, topographic data can be taken into account. The results of inversion consist in pseudo geoelectric sections (resistivity calculated according to the depth) but are not defined in a unambiguous way. The electrical resistivity depends on several soil properties and can be used i) to characterise the texture of the soil, especially its clay content of soil (Fukue et al., 1999; Giao et al., 2003), ii) to describe the pore geometry especially with the help of the Archie's law (Archie, 1942), iii) to measure the soil water content (Binley et al., 2002) and its temporal variation, and iv) to discuss the salinity of the soil or the composition of the soil solution (Rhoades et al., 1977; Kalinski et Kelly, 1993). In the field, 2D or 3D tomographies enable to describe the variation of soil porosity or soil density (Robain et al. 1996; Besson et al., 2004) and the evolution of the water content (Aaltonen, 2001; Binley et al., 2002; Michot et al., 2003; Zhou et al., 2003).

Recent technological improvements have consisted in building automatic profilers that can be used in the field for prospecting areas up to a few hectares: this technology is now operational and consists in a continuous multi-depths electrical resistivity profiler, called MUCEP (Panissod et al., 1997). This system comprises a multi-probe system pulled by a cross-country vehicle. The device is composed of three arrays, called the V1 array, the V2 array and the V3 array. Each array is composed of four wheels that are metallic probes with two Ci electrodes to inject current in the soil, and two Pi electrodes to record the soil electrical potentials. The spacings between the current probes and the potential probes are 0.5 m for the V1 array, 1.0 m for the V2 array and 2.0 m for the V3 array. The electrical measurements consist of bulk electrical resistivities and the volume of soil investigated depends on the array geometry. Former studies have shown that the depth of the soil volume investigated is of the order of magnitude of the spacing between the electrodes (Dabas & Tabbagh, 2003). The apparent electrical resistivity is measured for three pseudo-depths and its interpretation helps in delineating different soils in digital soil mapping, without any inversion of the signal (Bourennane et al., 1998; Tabbagh et al., 2002).

Another interesting method consists in The Geometrics OhmMapper as a capacitively-coupled resistivity meter that measures the electrical properties of rock and soil with investigation depth of 2-3m without cumbersome galvanic electrodes used in traditional resistivity surveys. A simple coaxial-cable array with transmitter and receiver sections is pulled along the ground either by a single person or attached to a small all-terrain vehicle (Figure 5). Thus, data collection is many times faster than systems using conventional resistivity surveys devices (Yamashita et al., 2005). Interpretation is based on inversion of the signal.

a)   **b)**

Figure 5: a) conventional resitivity survey device, b) OhmMapper console and antenna array

2.2.3. Strengths and limitations

Geoelectrical resistivity measurements refer to relatively well-known techniques. Soil properties that can be identified from geoelectrical data will therefore need limited further research. Nevertheless several problems still limit the interpretation of electrical resistivity measurements in terms of soil properties: 1 - with the commercial software, the inversion of apparent data diverges in case of sharp variations of apparent electrical resistivity values; this situation is really common when the soil dries and when cracks develop at the soil surface, even for clay content below 20 %. The interpretation of electrical resistivity in terms of soil bulk density is then difficult but a recent model can be improved to interpret the soil bulk density for cracked soils (Tabbagh et al., 2007). 2 - the electrical resistivity signal is influenced by several soil properties at the same time, which limits its interpretation in one property (see for example the effect of bulk density and water content, two properties of interest in our project). 3 - The resolution of the interpreted signal decreases versus depth and is usually not precise enough to describe the soil horizons. Other geophysical techniques have then to be taken into account for that interpretation or for joined inversion.

Concerning the expected progress in the context of DIGISOIL, the electrical resistivity is supposed to help in characterizing: the soil nature, the soil bulk density and the soil hydrologic characteristics by interpreting the variation of water content with time and depth. We have to i) produce a hierarchy between these different parameters according to each soil context or soil threat, and ii) propose relationships between electrical resistivity values and soil properties. Main tasks do not concern the development of new sensors but the improvement of methods used to interpret the experimental data obtained by the actual geoelectric technology too.

2.2.4. Available commercial sensors

Key features of commonly used resistivity systems are presented in Table 2. More detailed sheets of comparison can be found in Appendix A.

Instrument		Measurement				Transmitter Output			IP Windows	
						Power (W)	Current (mA)	Max Voltage	# of Windows	User Defined
Mark	Model	Resistivity	IP	SP	# of Channels					
ABEM	Terrameter LS	☑	☑	☑	4 or 12	250	2500	± 600 V	Arbitrary	☑
	SAS 4000 + ES10-64	☑	☑	☑	4	100	1 - 1000	± 400 V	10	☑
	SAS 1000 + ES10-64E	☑	☑	☑	1	100	1 - 1000	± 400 V	10	☑
AGI	SuperSting R8 IP	☑	☑		8	200	1 - 2000	± 400 V	6	☑
	SuperSting R1 IP	☑	☑	☑	1	200	1 - 2000	± 400 V	6	☑
	MiniSting + SWIFT	☑	☑	☑	1	no info	1 - 500	± 400 V	6	☑
	Marin	☑	☑		8	200	1 - 2000 *	± 400 V	6	☑
IRIS	Syscal Pro Switch 48/72/96	☑	☑	☑	10	250/1200**	2500	± 800/1000 V	20	
	Syscal Pro Deep Marin	☑	☑	☑	10	2000	40000	56 V	no info	no info
	Syscal R2	☑	☑	☑	1	250/1200**	2500	± 800 V	4	
	Syscal R1 Swich 48/72	☑	☑	☑	1	200	2500	± 600 V	4	
	Syscal Junior Swich 48/72	☑	☑	☑	1	100	1200	± 400 V	4	☑
	Syscal Kid Swich 24	☑		☑	1	25	500	± 200 V	N/A	N/A
GF	ARES	☑	☑	☑	1	300	2000	± 550 V	10	
Scintrex	SARIS	☑	☑	☑	1	100	1000	± 500 V	4	☑
PASI	16gl	☑			1	450	500	± 900 V	N/A	N/A
Allied (Campus)	Tigre	☑		☑	1	18	0.5 - 200	± 180 V	N/A	N/A

* 1 - 1250 in land
** with Generator

Table 2 : List of known manufacturers for geoelectric instruments and associated specifications.

2.2.5. Available non-commercial sensors

Table 3 list the specifications of the non-commercial sensor developed by INRA and CNRS and that will be used in the project.

Devices	Manufacturers	Specifications
Multi-depths electrical resistivity profiler MUCEP	Eurocim - CNRS INRA	Multi-probe system pulled by a cross-country vehicle
		Input voltage : 12V DC Output current : 10 mA or 20 mA with a frequency of 122 Hz
		Resistivity meter RMCA.4
		3 operating range : 0-200 Ω ; 0-2 kΩ ; 0-20 kΩ
		Doppler radar for measurement every 10 cm (progression of vehicle)
		Steel electrodes distribute around 4 pairs of metallic wheels: One pair for current injection Three pairs for electrical potentials measurement

Table 3 : List of known manufacturers for geoelectric instruments and associated specifications.

2.3.   ELECTROMAGNETIC INDUCTION

2.3.1. Measurement principles

Electromagnetic induction (EMI) uses the propagation of electromagnetic fields through the soil to measure its electrical properties, more particularly the electrical conductivity. The measurement principle of this technique is illustrated in Figure 6. A very low frequency (1-100 kHz) alternating current passing through a transmitter coil antenna generates a primary alternating magnetic field. This variable primary magnetic field propagates into the soil and, in accordance with Faraday's law, induces circular loops of alternating eddy-currents, which intensity is proportional to the soil electrical conductivity. The current loops produce an induced alternating magnetic field proportional to the intensity of the current. The primary and the induced magnetic fields combine and form a secondary magnetic field which in turn induces an alternating current within a receiver coil antenna. The amplitude and the phase of the secondary magnetic field differ from those of the primary magnetic field. The comparison of the emitted and recorded signals allows retrieving the electrical conductivity of the soil. Some EMI sensors are equipped with one or two additional 'bucking' coil(s) used to avoid transmitter-receiver mutual coupling, resulting in an improved sensitivity of the system.
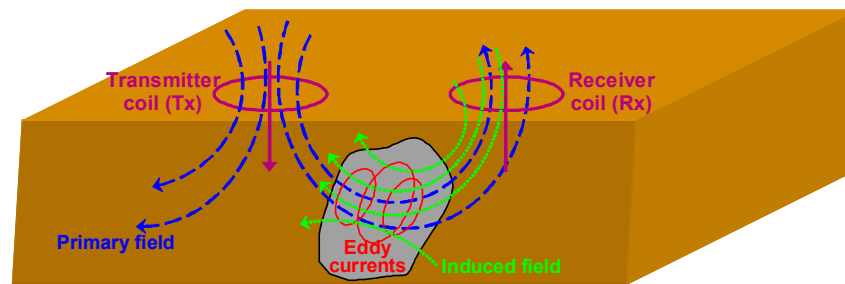
Figure 6. Measurement principle of soil electrical conductivity with electromagnetic induction.

Considering coils as magnetic dipoles, several configurations may be distinguished for EMI devices as a function of the orientation of the antennas with respect to the subsurface: horizontal (i.e., dipole parallel to the subsurface) transmitter and receiver (H-H), vertical (i.e., dipole perpendicular to the subsurface) transmitter and receiver (V-V) and vertical transmitter with horizontal receiver (V-H) modes exist. Antenna orientation influences the relative sensitivity of the signal to electric properties as a function of depth. The sensitivity of H-H and V-H modes is very high for shallow layers and it decreases sharply with increasing depth. In contrast, the V-V mode is insensitive at the surface but its sensitivity increases rapidly with depth, reaches a maximum value and then decreases similarly as the other modes (McNeill 1980; Wait 1962). As a result, combining EMI measurements obtained from the different modes would provide information regarding variation of electrical conductivity with depth. Moreover, EMI systems also differ by the distance separating the transmitter and the receiver coils.

2.3.2. State-of-the-art and applications

Soil electrical conductivity is influenced by several physico-chemical factors, namely water content, mineralogy, texture, porosity, salinity, structure, temperature, cation exchange capacity, organic matter and bulk density (Corwin and Lesch 2005; Friedman 2005). As a result, EMI soil electrical conductivity measurements have been used in numerous studies in order to assess one or some of these properties at the field scale, as well as to investigate processes related to their spatial and/or temporal variability. The use of EMI in soil science has been initiated by de Jong et al. (1979) for soil salinity surveys. Since then, EMI has been used for the same purpose (Bennett and George 1995; Hendrickx et al. 1992; Lesch et al. 1995a; Lesch et al. 1995b; Wollenhaupt et al. 1986) as well as for a wide range of other environmental applications, which includes soil water content measurements (Freeland et al. 2001; Kachanoski et al. 1988; Khakural et al. 1998; Sheets and Hendrickx 1995), evaluation of groundwater recharge (Cook and Kilty 1992; Cook et al. 1992; McNeill 1991), detection of contaminants in soils and shallow aquifers (Eigenberg and Nienaber 1998; Greenhouse and Slaine 1983; Hoekstra et al. 1992; Siegrist and Hargett 1989; Stevens et al. 1995), location of clay layers in soil (Cockx et al. 2007; Doolittle et al. 1994), determination of the spatial variability of soil texture (Anderson-Cook et al. 2002; Doolittle et al. 2002; Williams and Hoey 1987) and assessment of cation exchange capacity (Dunn and Beecher 2007; McBride et al. 1990). Archaeological surveys (Bongiovanni et al. 2008) and detection of buried landmines (Scott 2007) are also other practical applications of EMI.

Regarding data processing, several approaches have been developed to infer investigated soil properties from EMI measurements. A first approach, presented by McNeil (1980), is based on the assumption of a linear relationship between the soil electrical conductivity and the ratio of the quadrature components of the secondary and the primary magnetic fields. This approach provides reliable evaluations of the electrical conductivity of the soil for low values of the induction number, defined as the ratio between transmitter-emitter coil spacing and the skin depth (i.e., the depth at which the primary magnetic field has been attenuated to 1/exp of its original strength). Furthermore, it assumes uniform soil conductivity in the vertical direction and measurements correspond therefore to apparent soil conductivity, i.e., depth-weighted average of soil electrical conductivity. Cook and Walker (1992) adapted this model to account for depth distribution of electrical conductivity, combining measurements obtained from different configurations (i.e., transmitter-receiver orientation, spacing and height above ground). Borchers et al. (1997) also extended the model of Mc Neill (1980) using second order Tikhonov regularization inverse procedure to estimate conductivity profiles. A more sophisticated – nonlinear – model has also been developed, it accounts for vertical variation of soil conductivity and it is applicable for high values of the induction number (Ward and Hohmann 1987).

Numerous other approaches are based on the modelling and inversion of solutions for two-dimensional (2-D) or three-dimensional (3-D) Maxwell's equations, governing the behaviour of electromagnetic fields in a multilayered medium. These approaches are expected to provide better description of the actual feature of the soil than those presented above which consider the subsurface as a one-dimensional (1-D) system. Nevertheless, their development and use only became significant during the last decade as a result of the high computation costs of these techniques. Pioneer works in this field presented solutions for 2-D or 3-D bodies with simple geometry and embedded in uniform or layered 1-D media (Lee and Morrison 1985; Lee et al. 1981; Stoyer and Greenfield 1976). Later, methods were developed to obtain numerical solutions allowing to consider more general 2-D and 3-D models. The most commonly used methods may be classified in to three categories. The first type is the Finite-Difference methods in which the conductivity, the electromagnetic fields and the Maxwell's differential equations are approximated by their finite-difference counterparts within a rectangular 2-D or 3-D grid (Fomenko and Mogi 2002; Newman and Alumbaugh 1995; Newman and Alumbaugh 1997; Sasaki 2001; Weaver et al. 1999); the main attraction of this method is the simplicity of its numerical implementation. The second kind of approaches is the Finite-Element in which the electromagnetic field is decomposed into some basic functions (Badea et al. 2001; Mitsuhata 2000; Mitsuhata et al. 2002; Unsworth et al. 1993; Zunoubi et al. 1999); compared with the other approaches, the finite-element method would better account for geometry but the construction of the finite element is nontrivial and generally time-consuming. Thirdly, the Integral Equation methods reduce the differential Maxwell's equations into an integral equation, called the scattering equation (Cerv and Pek 1990; Dmitriev and Nesmeyanova 1992; Xiong 1992; Xiong and Tripp 1995). Besides, approximates solutions have also been developed, such as thin sheet solutions (Dawson and Weaver 1979; McKirdy et al. 1985; Vasseur and Weidelt 1977) and artificial neural network solutions (Poulton and Birken 1998; Spichak and Popova 2000), which impose

additional constrains on the conductivity models and/or the electromagnetic field behaviour.

2.3.3. Strengths and limitations

As stated above, soil electrical conductivity integrates several factors which makes EMI useful for a wide range of environmental applications. Moreover, EMI is non invasive and individual measurements are almost instantaneous. As a result, EMI is a relevant technique for characterizing large areas with fine spatial and/or temporal resolutions, using time-lapse measurements in the latter case. Nevertheless, besides these advantages, current EMI systems also present some limitations. One disadvantage relies in the dependency of soil electrical conductivity on several factors, which may make the interpretation of the signal variation rather complex if more than one influencing soil properties vary at the same time. Moreover, EMI usually operates at a single or at some fixed frequencies, which limits the information retrieved from the subsurface. In addition, the calibration of the existing sensors is generally rather empirical and not accurate, which reduces the reliability of the data. Furthermore, data processing used to retrieve soil properties from EMI techniques is sometimes only valid under restricted conditions (e.g., low induction number) and it also often relies on strong simplifying assumptions with respect to the antenna radiative properties or to the wave propagation phenomena. Finally, inversion procedures of EMI data may lead to inaccurate results as a result of uniqueness and stability issues in the inverse problem.

The use of Vector Network Analyzer (VNA) technology, as proposed in the framework of this project, would overcome a part of these limitations, allowing to work simultaneously at a wide range of frequencies as well as to perform standard, robust and reproducible, calibration. Moreover, adapting to EMI the approach developed by Lambot et al. (2004a,b) for GPR, will allow accurate characterization of the radiative properties of the antenna as well as full-waveform modeling of the soil response on the basis on the exact solution of the 3-D Maxwell's equations for wave propagation in a horizontally multilayered medium. Finally, inversion issues may be avoided by constraining the inverse problem through joined inversion of EMI measurements with data from other geophysical techniques (e.g., GPR, seismic) and/or integrating additional sources of information (e.g., hydrodynamic laws, hydropedology, …) in the inversion procedure.

2.3.4. Available commercial and non-commercial sensors

Manufacturer	Designation	Operating frequency(ies) (kHz)	Operating mode[1]	Conductivity range (mS m⁻¹)	Dimensions (m)	Tx-Rx spacing (m)	Exploration depth (m)	Weight (kg)
Geonics	EM31-MK2	9.8		10, 100, 1 000	4.0	3.66	6.0	12.4
	EM34-3	0.4 1.6 6.4	H-H, V-V	10, 100, 1 000	Receiver console: 0.19×0.135×0.26 Transmitter console: 1.55×0.08×0.26 Coils: 0.63 diameter	40.0 20.0 10.0	up to 60.0	20.5
	EM38	14.6	H-H, V-V	1 000	1.06×0.15×0.036	1.0	H-H: 0.75 V-V: 1.5	6.8
	EM39 (borehole)	39.2		100, 1 000, 10 000	1.63 × ∅=0.036	0.5	500	2.2
Dualem	Dualem-1S	9.0	V-V, V-H	3 000	1.41 × ∅=0.09	V-V: 1.0 V-H: 1.1		5
	Dualem-2		V-V, V-H			2.0		
	Dualem-4		V-V, V-H			4.0		
	Dualem-21S		V-V, V-H			1 and 2		
	Dualem-42S		V-V, V-H			2 and 4		
	Dualem-421S		V-V, V-H			1, 2 and 4		
GSSI	Profiler	1 to 16 max. 3 freq. simultaneously	H-H, V-V		1.46×0.24×0.124	1.22		4.5
Geophex	GEM-2	0.3 to 96	H-H, V-V		1.83×0.125		20-30	2.0
	GEM-2A	0.33 to 96	H-H, V-V		6.43	V-V: 5.1 H-H: 5.92		110
	GEM-3	0.3 to 96	V-V		∅=0.3, 0.4, 0.64, 0.96			

[1]H-H: transmitter and receiver horizontal dipole orientation; V-V: transmitter and receiver vertical dipole orientation; V-H: vertical transmitter and horizontal receiver dipole orientation

Table 4 : List of known manufacturers for EMI devices and associated specifications.

2.4. MAGNETISM

2.4.1. Measurement principles

The measurements principles are almost the same as the EMI ones. In fact, the properties measured are the magnetic susceptibility, which is the capability for the soil to acquire i) an induced magnetization in a weak magnetic inducting field and ii) a magnetic viscosity that characterizes the delayed acquisition or loss of an induced magnetisation when an inducing magnetic field is applied or shut off. The kinds of geometries used for the measurement are the same as in EMI but it always respects the low induction number condition (Mullins 1974, Tabbagh 1986a). Thus, the investigation depth is mainly dependent on the transmitter-receiver distance.

2.4.2. State-of-the-art and applications

As the human activities may change the magnetic properties of soil, the first uses were for archaeological purposes (Colani and Aitken 1966, Tite and Mullins 1971, Tabbagh 1986b). Then with the development of environmental magnetism (Thomson and Oldfield 1986), the measurements of magnetic properties have been applied to characterize land pollution and to differentiate loess from soils in palaeoclimatic studies (Heller and Evans 1995, Liu et al. 2005). The spatial variations of magnetic properties are mainly driven by pedogenesis, transfer, bacterial or human activity (Marmet et al

1999). Though there are a lot of EMI sensors available, most of them only measure the apparent conductivity. Mostly used in environmental magnetism studies, the MS2 from Bartington Ltd presents the advantages of field measurements with the MS2D probe and laboratory measurements with the MS2B sensor. The Geonics EM38B, allowing the simultaneous measurement of the in phase and quadrature phase component is interesting too. In addition to these devices, the UMR 7619 Sisyphe have developed various slingram prototype like the CS60 (Job et al. 1995), which permits the simultaneous measurement of magnetic susceptibility and electrical conductivity. The magnetic viscosity, though well known as a phenomenon, has not been measured until recently with the release of the MVM with probes very similar to the ms2 and the VC100 (Thiesson et al. 2007) a slingram device, both measuring the magnetic viscosity. As the depth of investigation is link to the transmitter receiver spacing, it must be underlined that the 1m spacing of the EM38 is commonly too great for soil electrical conductivity studies but it will be suitable for magnetic susceptibility measurements. The Dualem 21s with its four-coil configuration appears to be interesting too though it got a 2m spacing which will probably be too great for studying soils. All this systems have data logger and the measurements are fast.

2.4.3. Strengths and limitations

The measurements of magnetic susceptibility with EMI device are fast and can be simultaneous with the electrical conductivity ones. The transmitter and receiver coils do not necessitate direct contact with the soil. As the measurement are possible only under the low induction number assumption, the depth of investigation is limited by the receiver-transmitter spacing. The need of mechanical rigidity makes the measurement of magnetic susceptibility more difficult. In fact, a thermal drift would have to be corrected on most devices. In addition, except for the MS2, all the in phase measurement are given in ppm and have to be transformed in apparent magnetic susceptibility. For the magnetic viscosity measurements, there is no mechanical constraint but as the emitted field is a pulse, there are more sensible to electromagnetic noises. The only mean to investigate the varying of the magnetic properties with depth is to have either several devices with different geometries or one device with several receivers and inter-coil spacing.

The expected progresses in the context of DIGISOIL are mainly on the meanings of the variation of magnetic properties in soils in term of texture and to propose relationship between soil properties and apparent magnetic properties values. Another point is to determine a reliable process for measure the magnetic properties with commercial devices or prototypes. The simultaneous use of MS2D, CS60 and EM38 (Or DualEM21S) will constitute a suitable combination to record the vertical variation of the magnetic susceptibility. The main tasks will be on improving the existing sensors and the way to use it to measure the magnetic properties

2.4.4. Available commercial and non-commercial sensors

Devices	Manufacturers	Specifications
MS2	Bartington ltd	with the MS2D field probe Working frequency : 958Hz Ø 0.18m
EM38B	Geonics ltd	HCP or VCP
		Working frequency :14.6kHz
		Intercoil spacing: 1m Simultaneous measurements in phase and in quadrature of phase
		Perp and HCP
Dual EM 21S	dualem	Working frequency : 9kHz Intercoil spacing 1 : 1m HCP, 1.1m Perp Intercoil spacing 2 : 2m HCP, 2.1m Perp Simultaneous measurements in phase and in quadrature of phase
CS60		VCP or HCP
		Working frequency : 27.96kHz
		Intercoil spacing : 0.6m Simultaneous measurements in phase and in quadrature of phase
MVM	Pulsepower	With the D field probe Various time sampling(10, 15, 20, 25, 30, 35, 40,45, 50, 60, 70, 80, 90 and 100µs) Ø 0.18m
VC100		Perp Samples at 12.2, 22.9,44.1,87.9,176µs after pulse shut off Intercoil spacing : 1m

Table 5 : List of known manufacturers for magnetic instruments and associated specifications

2.5. GROUND PENETRATING RADAR

2.5.1. Measurement principles

GPR is a geophysical technique which is particularly appropriate to image the soil in two or three dimensions with a high spatial resolution, up to a depth of several meters. GPR operates by transmitting high frequency (VHF-UHF, i.e., 10-2000 MHz) electromagnetic waves into the soil (see Figure 7). Wave propagation is governed by the frequency-dependent soil dielectric permittivity ε (determining wave velocity), electric conductivity σ (determining wave attenuation), magnetic permeability μ (determining wave velocity, affects attenuation), and their spatial distribution. Electromagnetic contrasts create partial wave reflections and transmissions that are measured by a receiving antenna, depending on the mode of operation (reflection or transmission). For non-magnetic materials as prevalent in the environment, μ is equal

to the free space magnetic permeability μ_0 and, thereby, does not affect wave propagation compared to free space conditions.

The main characteristic of a GPR system is its operating frequency (centre frequency), determining resolution (typically considered as one quarter the wavelength) and penetration depth. Penetration depth is also determined by the electrical losses in the ground and scattering phenomena. The choice of an operating frequency is always a trade-off between resolution and penetration depth, as higher frequencies permit higher resolution but lower penetration depth. When the antennas a coupled with the ground, dipole- and bowtie-type antennas are commonly used. For off-ground GPR, horn antennas a mostly used as they are more directive. Finally, antennas can be lowered in boreholes for both transmission and reflection measurements. Dipoles are then used as they geometrically extend in one dimension only. A radar system can use a single antenna as transmitter and receiver (monostatic mode), both a transmitting and a receiving antenna (bistatic mode, the most used), or several transmitters and receivers (multichannel systems). This last mode can be emulated by a bistatic system and by performing measurements with different antenna separations or positions. In that case, measurements are more time consuming. Multi-offset measurements provide more information compared to single offset measurements. There are two families of GPR: the time domain systems, also called pulse radars, and the frequency domain systems. The time domain radars are by far the most commonly used. They are based on the transmission of a pulse in the time domain. The frequency domain systems transmit stepped-frequency continuous-waves and are increasingly used nowadays, not only because electronic components become more affordable, but also because it presents a series of advantages compared to pulse radars.
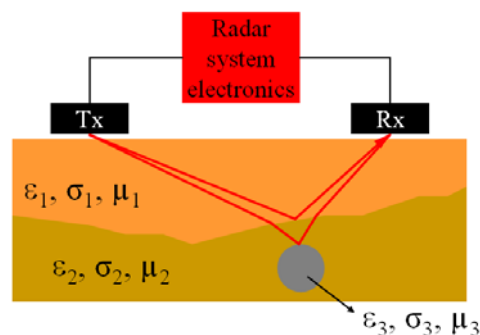
Figure 7: Ground penetrating radar (GPR) basic principles. Tx is the transmitting antenna. Rx is the receiving antenna. Slid lines represent wave propagation paths (straight-ray approximation).

First GPR applications started in the 60s, mainly for geological surveys. In the 70s, the first commercial GPR systems were available and introduced in civil and military engineering, as well as in archaeology. In the 80s, GPR was introduced in forensic investigations. In the 90s, first researches and applications were initiated in agricultural and environmental engineering. Most GPR surveys were mainly focused on qualitative imaging of the subsurface. During the last decade, considerable efforts have been devoted to GPR for more quantitative analyses, thereby providing information regarding the soil properties and their spatial distribution. Progress in the technology

itself has been made by progressively improving the dynamic range of the systems and efficiency of the antennas, speed of acquisition, and real-time user interfaces including visualization and basic processing of the radar images. Modern systems also include multi-channel acquisition.

Figure 8 illustrates a GPR image of the subsurface, where measurements have been made along a transect. The profile is recorded with a PulsEkko 1000 system (Sensors & Softwares Inc.) using fixed offset 250 MHz centre frequency shielded antennas with a transmitter-receiver separation of 25 cm. The horizontal step size was 5 cm and a time step of 0.2 ns was used. The recording is made in the central part of the Netherlands in a partial consolidated sand environment with an unconsolidated top layer.
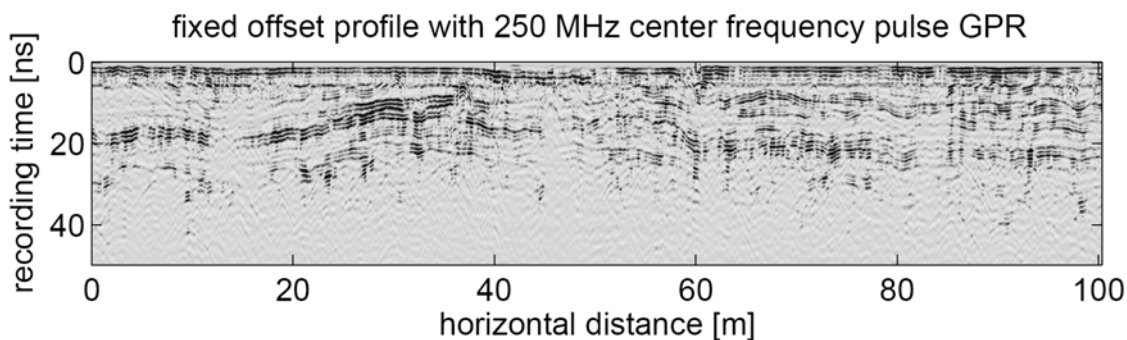
Figure 8: GPR image of the subsurface, illustrating soil stratigraphy up to a depth of about 5 meters (Courtesy Evert Slob).

2.5.2. State-of-the-art and applications

GPR has been primarily used to image the subsurface and detect buried objects. In the areas of unsaturated zone hydrology and water resources, GPR has been used to identify soil stratigraphy (Boll et al., 1996; Davis and Annan, 1989; Grandjean et al., 2006; Grandjean et al., 2001), to locate water tables (Nakashima et al., 2001), to follow wetting front movement (Vellidis et al., 1990), to identify soil hydraulic parameters (Binley et al., 2002; Cassiani and Binley, 2005; Kowalsky et al., 2005; Lambot et al., 2004a), to measure soil water content (Chanzy et al., 1996; Galagedara et al., 2005a; Huisman et al., 2003; Huisman et al., 2002; Lunt et al., 2005; Serbin and Or, 2004), to assess soil salinity (al Hagrey and Müller, 2000), to monitor contaminants (Yoder et al., 2001), and to delineate soil compaction within agricultural fields (Petersen et al., 2005). Time-lapse GPR measurements have recently permitted to monitor soil water dynamics between boreholes and infer the soil hydraulic properties governing water flow (Binley et al., 2001; Cassiani and Binley, 2005; Kowalsky et al., 2005; Linde et al., 2006; Rucker and Ferré, 2004; Tsoflias et al., 2001). Shallow soil unsaturated hydraulic properties can also be obtained from off-ground radar data (Jadoon et al., 2008; Lambot et al., 2006a). GPR can be applied to monitor remediation amendments and processes, provided sufficient sensitivity of the GPR signal to these changes (Hubbard et al., 2005).

The choice of a particular GPR system or setup depends on the application, information that is intended to be retrieved, and processing algorithm that is intended to be used. Generally, GPR signal analysis is performed using ray-tracing approximations (see Figure 7 and Figure 9) and tomographic inversion. Several methodologies are generally adopted for determining wave propagation velocity and retrieve corresponding soil dielectric permittivity and correlated water content from the GPR data (Huisman et al., 2003) :

- Determination of the wave propagation time to a known interface using single-offset surface GPR (Grote et al., 2003; Lunt et al., 2005; van Overmeeren et al., 1997; Weiler et al., 1998);

- Detection of the velocity-dependent reflecting hyperbola of a buried object using single-offset surface GPR along a transect (Vellidis et al., 1990; Windsor et al., 2005);

- Extraction of stacking velocity fields from multi-offset radar soundings at a fixed central location (common midpoint method) (Garambois et al., 2002; Greaves et al., 1996);

- Determination of the ground-wave velocity for surface water content retrieval using multi- and single-offset surface GPR (Chanzy et al., 1996; Du and Rummel, 1994; Galagedara et al., 2003; Galagedara et al., 2005a; Galagedara et al., 2005b; Grote et al., 2003; Huisman et al., 2002; Huisman et al., 2001);

- Determination of the surface reflection coefficient using single-offset off-ground GPR (Chanzy et al., 1996; Redman et al., 2002; Serbin and Or, 2003; Serbin and Or, 2004);

- Determination of the two-dimensional spatial distribution of water between boreholes using transmission tomography (Alumbaugh et al., 2002; Binley et al., 2001; Rucker and Ferré, 2005; Zhou et al., 2001).
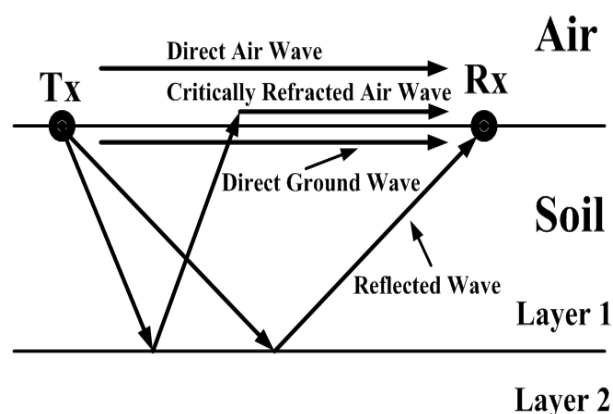
Figure 9: Propagation paths of GPR waves in a two-layered soil.

2.5.3. Strengths and limitations

Although these GPR techniques are well established, they still suffer from major limitations originating from the strongly simplifying assumptions on which they rely with respect to electromagnetic wave propagation phenomena. As a result, a bias is introduced in the estimates due to limited GPR model adequacy and, moreover, only a part of the information contained in the radar data is used, generally the propagation time. In addition, all these techniques are not appropriate in a real-time mapping context, as usually several measurements are needed at a given location to increase information content in the data. Recent progress with multi-channel systems partly permits to palliate at that last shortcoming.

Resorting to the physical basis of GPR wave propagation is necessary to estimate simultaneously both the depth dependent soil dielectric permittivity and electric conductivity. The relation between the subsurface constitutive parameters and the measured electromagnetic field is governed by Maxwell's equations. Reconstruction of the unknown constitutive parameters from the known field appeals to inverse modelling. Inverting electromagnetic data has been a major challenge in applied geophysics for many years. Successful inversion is challenging since it involves rigorous forward modelling of the 3-D GPR-subsurface system, which is furthermore computationally very time-consuming (Ernst et al., 2007; Gloaguen et al., 2007; Lambot et al., 2008; Sasaki, 2001; Solimene et al., 2007). Moreover, the inverse problem should satisfy uniqueness and stability conditions, which are related to the information content in the radar data.

Technically, beyond the complexity of advanced signal processing methods, these limitations originate also from the commercial radar systems themselves, for which the measured quantity can not be fully described due to the absence of robust calibration techniques for the instruments. As an example, the definition of time zero in the data is already subject to large uncertainties for time domain systems (Yelf, 2004).

2.5.4. Available commercial and non-commercial sensors

Several manufacturers commercialize GPR systems nowadays. The oldest company is GSSI, which is the most important one present on the market, for both applications and research. All manufacturers propose a range of different antennas operating at different frequencies, from a few MHz to the GHz frequencies. Table 6 presents a list of the main GPR manufacturers, including the name of their radar products, and some key notes (not exhaustive list). The GSSI, Sensors & Softwares, and Mala equipments are the most used in research by universities and research institutions and for agricultural/environmental engineering applications. Other companies are more dedicated to civil engineering applications (e.g., concrete inspection, buried pipe detection, etc.). All available GPR systems are time domain radars (pulse radars), except for 3d_Radar who proposes two stepped-frequency continuous-wave systems.

Frequency domain radars can be readily set up using vector network analyzer (VNA) technology. A series of VNA manufacturers exist and the two main ones are Rohde & Schwarz and HP Agilent, each proposing a series of different systems. These systems

are not listed here as they can not yet be considered as GPR systems (their scope is not initially intended for such applications and they are presently used in GPR research only).

Manufacturer	Radar system	Key characteristics
GSSI	SIR-20	Antennas in the range 15-2600 MHz 2 channels
	SIR-3000	1 channel
Sensors & Software Inc	**PulseEKKO PRO**	Antennas: 12.5-1000 MHz 1 channel
	Noggin	Antennas: 250-1000 MHz
MALA GeoScience	RAMAC (X3M, ProEx, CX)	Antennas in the range 25-1000 MHz
	MIRA	Antenna array: 200, 400, 1300 MHz Up to 16 channels
IDS	RIS ONE	Antennas: 25-2000 MHz
	RIS MF Hi-Mod	Multi-frequency array
3D-Radar AS	3d-Radar Antenna arrays	Frequency domain radar Antenna array : 100-2000 MHz
	GeoScope	Antennas: 30-2000 MHz
Utsi Electronics	Groundvue	Antennas : 30-4000 MHz
RASCAN Systems LLC	Rascan	Investigation depths : 15-35 cm
PipeHawk	PipeHawk II	

Table 6. List of GPR manufacturers and commercial products.

2.6. HYPERSPECTRAL

2.6.1. Measurement principles

The study of the light reflected by an object to determine its properties is the subject of a discipline named diffuse reflectance spectroscopy. This technique relies on the analysis of spectral reflectance, which can be described as the reflectance as a function of wavelengths. Reflectance is the "radiant power […] reflected from the surface of a system divided by the incident radiant power" (Sheppard et al., 1985). In other words, it expresses the percentage of incident light reflected from a surface. Near-InfraRed (NIR) spectroscopy was applied – since its first developments in the 1960's – to various fields of science like food and animal sciences, pharmaceuticals, chemicals, agronomy, textile, etc. (Davis, 1998). To a lesser extent, Visible (VIS) and Mid-InfraRed (MIR) parts of the spectrum have been used as well. The different regions of the electromagnetic spectrum and their spectral ranges are presented in Figure 10 and Table 7. Several classifications of the spectral regions exist, depending on the field of science (e.g. laboratory spectroscopy or hyperspectral remote sensing). The classification as defined in Table 7 is often used in remote sensing literature.

Every substance possesses its own characteristic spectrum that can be detected by a sensor. This spectrum constitutes a unique 'fingerprint', which is determined by the

composition of the object in question. The form of the spectrum in a particular wavelength region depends on the selective absorption of radiations at given frequencies by molecular bonds. The VNIR and SWIR regions are characterised by absorption bands due to overtones and combinations of the fundamental vibrations of bonds C-H, N-H and O-H in the Mid InfraRed (MIR) (Pasquini, 2003).
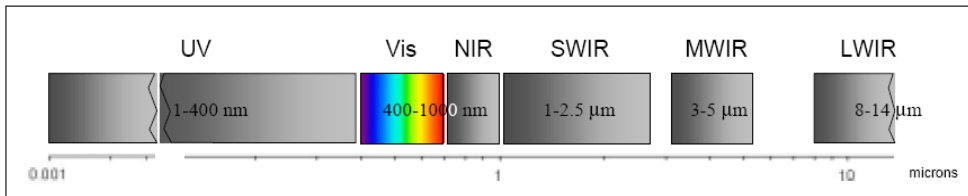
Figure 10: Typical Hyperspectral Frequency Bands.

Wavelength	Region of the electro-magnetic spectrum	Abbreviation
250 nm		
	Ultraviolet	UV
400 nm		
	Visible	VIS
700 nm		
	Near-Infrared	NIR
1.1 μm		
	Short Wave Infrared	SWIR
2.5 μm		
	Mid-Infrared	MIR
25n μm		

Table 7: Regions of the electromagnetic spectrum.

Spectral information can be acquired with various kinds of sensors, in the laboratory and in the field. The latter configuration implies that measurements are carried out under uncontrolled environmental conditions. One can classify spectral measurements in three groups: (i) point spectroscopy: spectra are measured one point at a time (e.g. with a contact probe in the laboratory), (ii) on-line spectroscopy: spectra are collected as an array of measurements (e.g. the sensor is mounted on a tractor and its position is recorded by a GPS receiver, see Mouazen et al., 2007), and (iii) imaging spectroscopy: spectra are recorded as a two-dimensional array of measurements (e.g. hyperspectral remote sensing with a whiskbroom or pushbroom scanner[1], see Ben-Dor et al., 2008a).

---

[1] A whiskbroom scanner consists of a single sensor using rotating mirrors to scan the surface. A pushbroom consists of a 2-dimensional sensor array, scanning the landscape directly for the entire width of the image.

The source of the incident radiation can be from natural or man-made sources. Hyperspectral sensors typically rely on solar radiation, and as a result require relatively cloud-free conditions during image-capture. These imagers capture the unique spectra, or "spectral signature", of an object, which can then be used to identify the material of which it is composed, much as a fingerprint can be used to identify a person. An often-used guideline to distinguish hyperspectral from multispectral sensors involves the capability of measuring 30 or more bands or channels in the electromagnetic spectrum. Therefore a Hyperspectral imager is defined to be one that can image at least 30 continuous spectral bands somewhere in the UV through LWIR spectra. Hyperspectral imagers produce vast quantities of data because of the number of bands simultaneously imaged. These data typically result in a "*hypercube",* which consists of a 3-dimensional image map. The region imaged is displayed along the x-y axis, and the spectrum of each pixel is displayed along the z-axis (see Figure 11). This ability to gather vast amounts of information provides both advantages and disadvantages. On the one hand this information will eventually evolve into a multitude of useful final products. On the other hand, these cubes have challenging data storage and download requirements. For example, a single 512-line x614-pixel integer-format Airborne Visible-Infrared Imaging Spectrometer (AVIRIS) image contains more than 140 megabytes of data.
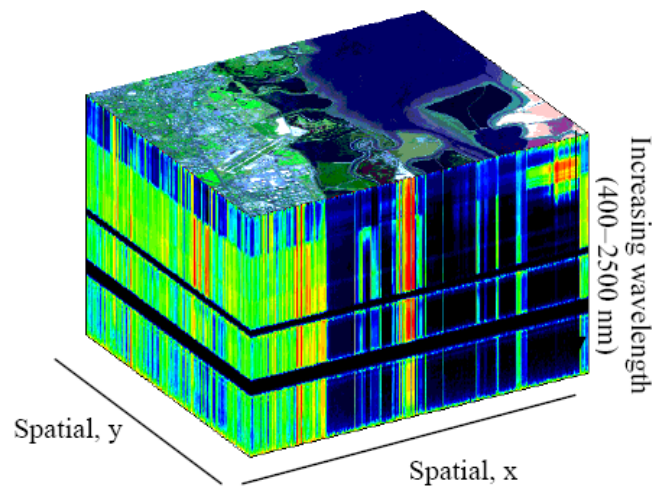
Figure 11: Typical AVIRIS Image HyperCube (Moffett Field, CA)

The spectral signature of an object is compared with an existing "spectral library" to determine its chemical composition and identity. Collection and calibration of the spectral library typically involves in-situ sampling and analysis. Both this cataloguing process and the image processing/ analysis steps are nontrivial, requiring significant future research and development. Improved software tools are needed for atmospheric corrections, multi-path reflections, and terrestrial calibration. Furthermore, exploiting hyperspectral technology continues to be a very labour-intensive endeavour. Airborne hyperspectral imagers have been available since the early 1980s. Spaceborne hyperspectral imagers to date have been, by and large, technology demonstrations,

and have not always been used for remote sensing. The NASA EO-1 Hyperion sensor is the first satellite to collect hyperspectral data from space (November 2000).

Qualitative interpretation of spectra through visual analysis can be achieved (see e.g. Stoner and Baumgardner, 1981). However, quantitative predictions require generally the use of complex statistical models. The development of such models is the subject of the discipline called *Chemometrics*. An overview on the use of chemometrics in spectroscopy, its history and main concepts has been published by Geladi (2003).

2.6.2. State-of-the-art and applications

Ben-Dor *et al*. (1999) and Malley *et al*. (2004) reviewed soil reflectance issues and applications. A brief overview on soil reflectance is given here. Soil reflectance in the VNIR range is characterized by absorption bands around 1.4 µm, 1.9 µm and 2.2 µm due to molecules known as 'chromophores' (Ben-Dor *et al*., 1997). If the shape of soil reflectance is relatively homogeneous across soil types in the 400-1000 nm region, the 1000-2400 nm region shows more pronounced differences in spectral shape (Ben-Dor *et al*., 1999). In general, soil reflectance decreases with organic matter concentration (Stoner and Baumgardner, 1981, see Figure 12). Although mineralogy (clay, iron oxides), organic matter and water constitute the main soil chromophores (Malley *et al*., 2004), other soil properties such as carbonate concentrations (Ben-Dor and Banin, 1990), CEC (Kariuki *et al*., 2003), dielectric properties (Middleton *et al*., 2004), soil texture (Sørensen and Dalsgaard, 2005), soil structural crusts (Ben-Dor *et al*., 2003), heavy metal contamination (Kemper *et al*., 2002), salt concentration (Farifteh *et al*., 2007), and soil nutrients (Na, P, K, S, Mg, Fe, Mn, etc.; e.g. Islam *et al*., 2003) have been studied as well. Due to its capacity to determine several soil properties simultaneously, VNIR spectroscopy has been applied successfully to build soil quality indicators (Idowu et al., 2008) and assess other soil functions or threats (Cécillon et al., 2008).
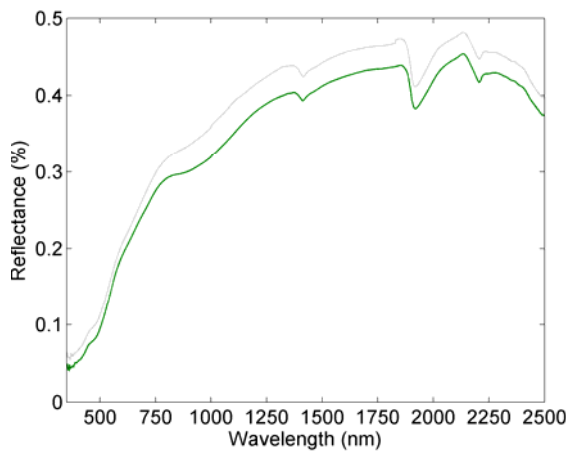
Figure 12: Spectral reflectance of two soil samples, with ± 1 % of organic matter (grey line) and ± 4.5 % of organic matter (green line).

Remote sensing of soil properties has been attempted with aerial photographs (Chen *et al.*, 2000; Fox and Sabbagh, 2002), multispectral (Galvão *et al.*, 2001; Chen *et al.*, 2005; Sullivan *et al.*, 2005), airborne hyperspectral images (Ben-Dor *et al.*, 2002; Uno *et al.*, 2005; Selige *et al.*, 2006) or spaceborne hyperspectral images (Gomez et al., 2008). Ben-Dor et al. (2008a) presented several successful case studies which have applied hyperspectral remote sensing to soil-related problems. Hyperspectral sensors differ from multispectral instruments in the greater number of wavebands, enabling a precise recording of the spectrum and a detailed analysis of spectral properties of the soil surface. Each pixel provides the full spectrum of the surface in the sensor range, giving the possibility to study spatial distribution of soil properties with a high spatial resolution. Using such sensors, several soil properties such as soil organic C (Ben-Dor *et al.*, 2002; Bajwa and Tian, 2005; Selige *et al.*, 2006; Stevens *et al.*, 2006; Stevens et al., 2008), total N (Selige *et al.*, 2006), clay content (Chabrillat et al., 2002; Selige *et al.*, 2006; Lagacherie *et al.*, 2008), soil moisture and electrical conductivity (Ben-Dor *et al.*, 2002), $CaCO_3$ content (Lagacherie *et al.*, 2008), dithionite extractable iron (Bartholomeus et al., 2007), salt content (Weng et al., 2008), biological soil crusts (Weber et al., 2008), soil drainage (Liu et al., 2008), pH, Ca, Mg, Na, K, bicarbonates and saturation percentage (De Tar et al., 2008) have been already investigated.

Soil Organic Carbon (SOC), as one of the main soil chromophores, has been particularly examined. Ben-Dor et al. (2002) obtained a R^2 of 0.83 between predicted and observed values of soil organic matter (SOM) in Israel clay soils using DAIS-7915 airborne data (400-2500 nm). Uno et al. (2005) and Stevens et al. (2006) obtained a R^2 of respectively 0.74 and 0.85 with the CASI airborne hyperspectral sensor (400-950 nm). Selige et al. (2006) achieved slightly better results (R^2 = 0.9) with the HyMap sensor (420-2480 nm). Less satisfactory prediction models of SOM were obtained by Bajwa and Tian (2005) with the RDACS/H-3 sensor (471-828 nm; R^2 = 0.66) and De Tar et al. (2008) with the AVNIR sensor (429-1010 nm; R^2 = 0.48). SOC predictions based on spaceborne sensors appeared also less accurate due to lower signal-to-noise ratio and spatial resolution, as showed by Gomez et al. (2008) with Hyperion images (R^2 = 0.51).

2.6.3. Strengths and limitations

There are three major constraints to the widespread use of imaging spectroscopy for soil applications (Ben-Dor et al., 2008a): (i) atmospheric absorptions interfering with the

signal, (ii) low signal-to-noise ratio and (iii) spatial variation in surface soil properties. These disturbing factors challenge the achievement of robust calibrations and repeatable results (Lagacherie et al., 2008; Stevens et al., 2008). The first category of constraints is caused by the distance between the sensor and the soil surface. Ben-Dor et al. (2004) examined the accuracy of several atmospheric correction methods. They found for instance that modelled reflectance values might in some cases differ up to 40 % from true reflectance. The second category of limitations is due the short integration time of the measurement over the target area. Chabrillat *et al.* (2002) showed in their study on the detection of expanding clays that the noise in hyperspectral data might be of the same amplitude as the spectral feature used to identify the type of clay. The last category of constraints is due to differences in samples preparation and conditions, which cannot be controlled outside the laboratory. In the field, spatial variation in soil surface properties (e.g. soil roughness, crusting, vegetation residue, moisture) and other chromophores (iron content, clay type) induces a spectral variability not directly related to the property studied. As a soil spectrum is the result of the overlapping of absorption features of several soil chemical and physical components, the relationship between single properties and soil spectra may not be straightforward.

Compared to other geophysical techniques, hyperspectral remote sensing can only measure the first few millimetres of the surface. As a consequence, such technique may be of little interest when strong vertical gradients in soil properties occur. Hyperspectral remote sensing should then be exploited in combination with other spectroscopic techniques, able to collect spectral data through the soil profile (see e.g. Ben-Dor et al., 2008b). However, the topsoil in cropland is well-mixed by ploughing and soil properties estimations by hyperspectral remote sensing can thus be extended to the plough layer.

2.6.4. Available commercial and non-commercial sensors

The recent and foreseen technology advancements promise an explosion in the quantity and quality of imaging remote sensing systems. The scientific and commercial communities become aware of allowance of unique hyperspectral imaging data acquisition opportunities. A brief profile of high resolution airborne hyperspectral sensor systems available for scientific and operational remote sensing activities is tried to be presented in this report. This overview covers multi- and hyperspectral civil, land and ocean nadir viewing observation sensors in the spectral range from the ultraviolet to the thermal infrared. A summary of the performance of each system is presented.

We are aware of several technologies for other systems (Acousto-Optical Tunable Filters, Time Domain Imaging Fourier Transform Spectrometer) that are not considered here. These systems lack definition and are in various stages of development. This review is limited to sensor-systems which are well documented and presently available to the international community for commercial or scientific purposes.

The sensors can be divided into two main different groups on the basis of the area covering:

- Wide field of view (FOV > 70°) devoted mainly to environmental and cartographic applications

- Low Field Of View (FOV < 70°) and a very low In Field Of View (IFOV) for scientific, simulating, and pre-space application tests.

Moreover, sensors can be divided into two main different scanning systems for acquiring the image:

- Whiskbroom imagers are working as electromechanical scanners. On-axis optics or telescopes with scan mirrors sweep from one edge of the swath to the other. The FOV of the scanner can be detected by a single detector or a single-line-detector. Simultaneously the movement of the airborne guarantees the sweeping scan over the earth. Well known example of whiskbroom imager are AVIRIS and MIVIS

- Pushbroom scanners, as electronical scanners they use a line of detectors to scan over a two dimensional scene, and in the case of two dimensional detector one dimension can represent the swath width (spatial dimension) and the other the spectral range. The number of pixels is equal to the number of ground cells for a given swath. The motion of the aircraft provides the scan in along-track-direction.

System	Spectral Range (nm)	Spectral Resolution (nm)	Across-Track Pixels x No. of Spectral Channels	FOV (°)	IFOV (mrad)	Dynamic Range
CASI-1500 Compact Airborne Spectrographic Imager ITRES Research *www.itres.com*	380 – 1,050	2.2	1,500 x 288	40	0.49	14
CASI-550 Compact Airborne Spectrographic Imager ITRES Research	400 – 1,000	<3.5	550 x 288	40.4	1.34	14
SASI-600 Shortwave Infrared Airborne Spectrographic Imager ITRES Research	950 – 2,450	15	600 x 100	40	1.2	14
TASI-600 Thermal Airborne Spectrographic Imager ITRES Research	8,000 – 11,500	125	600 x 32	40	1.25	14
MASI 600 Midwave IR Airborne Spectrographic Imager ITRES Research	3,000 – 5,000	32 av.	600 x 64	40	1.2	14
AISA EAGLE Specim *www.specim.fi*	400 – 970	2.9	1,024 x 488	30 or 37	0.5 or 0.64	12
AISA HAWK Specim	970 - 2500	8.5	320 x 254	18, 24, 35	0.94, 1.3, 1.94	14
AISA DUAL Specim	400 - 2500	2.9-8.5	320 x (499) or 1024 x 244(VNIR) + 320 x 254 (SWIR)	24 or 37 (VNIR) 35 (SWIR)	1.3 or 0.64 (VNIR) 1.94 (SWIR)	14

Table 8 : Pushbroom Hyperspectral Sensors.

System	Spectral Range (nm)	Spectral Resolution (nm)	Across-Track Pixels x No. of Spectral Channels	FOV (°)	IFOV (mrad)	Dynamic Range
AVIRIS Airborne Visible/Infrared Imaging Spectrom. JPL, CA *aviris.jpl.nasa.gov*	380 – 2,500	10	677 x 224	34	1	12 – 16
Hymap Integrated Spectronics *www.intspec.com*	450 – 2,500	15-20	512 x 128	35 – 60	2 x 2.5	12 – 16
Daedalus AHS-160 Argon ST *www.argonst.com*	450 – 12,700	30 (VNIR) 200(SWIR1) 16 (SWIR2) 300 (MIR) 400 (TIR)	750 x 80	90	2.5	12
Daedalus MIVIS Argon ST	433 – 12700	20 (VNIR) 50 (SWIR1) 9 (SWIR2) 360 (TIR)	755 x 102	71	2.0	12
DAIS 7915 Digital Airborne Imaging Spectrometer GER *www.op.dlr.de*	400 - 12600	15-30 (VNIR) 45 (SWIR1) 20 (SWIR2) 2000 (MIR) 900 (TIR)	512 x 79	52	3.3	16

Table 9 : Whiskbroom Hyperspectral/Multispectral Sensors.

2.7.   SEISMIC

2.7.1. Measurement principles

Seismic domain can be explored through different methods like seismic reflection/refraction (Lanz et al., 1998), surface waves analysis, cross-holes (Hayles et al., 1996), vertical seismic profile, tomography (Leblanc et al., 2004). For DIGISOIL purposes, the Spectral Analysis of Surface Waves (SASW) seismic method (Bitri et al., 1997) will be particularly detailed. This method is based on the principle of surface waves dispersion for the determination of shear waves velocity (Vs) in the first tens of metres of the under ground. The method allows obtaining a profile of velocity, in several points, for a cost widely lower than the destructive methods usually used in geotechnical (cross-holes). The necessary equipment for seismic measurements of surface waves consists in a seismic acquisition console, seismic sensors (geophones one or several components according to the recorded surface wave: Rayleigh or Love which propagate differently) regularly arranged along a linear profile and in an impulse source (hammer) (Figure 13, Figure 14).

Surface waves propagate in a parallel way at the surface of the Earth (Figure 15). In the case of a media of which the elastic properties vary with depth, surface waves velocity vary with the wavelength, and thus with the frequency. This effect is called dispersion. According to the considered frequency, surface waves contain the information about the propagation media between the surface and the maximal penetration depth of the different modes. By analyzing the dispersion of these waves, it is thus possible to obtain information about the values of physical parameters with

depths. The maximum of energy in the dispersion diagram permits to draw the dispersion curve which traduces the evolution of Vs with the frequency (Figure 15). These curves, as well as associated error bars, are then inverted from an a priori velocity model with the aim of reconstructing the vertical profile of shear waves velocity. The SASW method allows to measure the shear waves propagation velocity profile in the ground and consequently to determine the type of ground, and in the context of DIGISOIL, make an interpretation in term of soil compaction and bedrock depth.
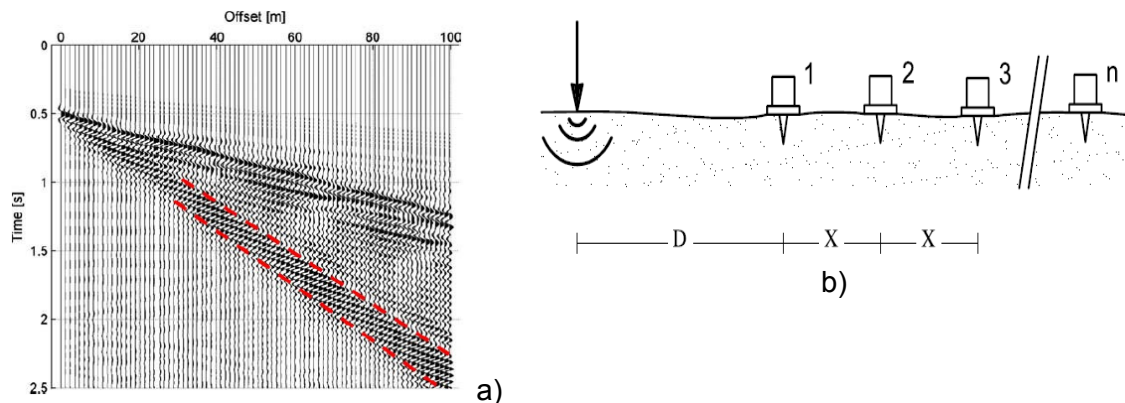
Figure 13 :a) Seismogram exemple for a 0 offset shot, surface waves appear between the red dotted lines, b) multistation array configuration for SASW measurments representing the impulse source (arrow) and geophones profile (Sebastiano Foti, 2000)

The length of the device and the minimum offset (distance between the source and the first receiver) are parameters mattering in the determination of the dispersion curve. In close field, plane waves estimation is not valid and transformations used to obtain the dispersion curves are not valid any more. In far field, meaning far offsets, the preferential attenuation of high frequencies leads an effect of pollution of short period part of our recordings by volume waves which perturb in this way the determination of dispersion diagrams. In the frequency range used in subsurface seismic survey, we cannot thus use too long profiles. In the context of DIGISOIL, device's length must be a compromise which allows us to have an optimal resolution in terms of wave number with a minimal length of profile.

a)

b)

Figure 14: a) Impulse seismic source photography, b) linear profile of seismic sensors photography.

a)

b)
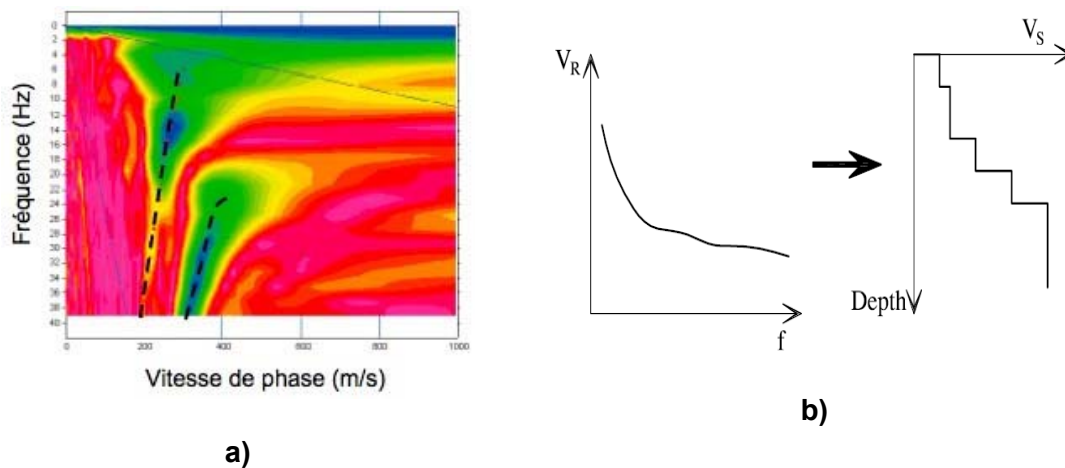
Figure 15: a) Exemple of dispersion diagram showing two propagation modes (dotted lines), b) schematic representation of inversion process (Sebastiano Foti, 2000).

2.7.2. State-of-the-art and applications

Due to the development of subsurface characterization studied for environmental purposes, the efficiency of seismic methods for estimating ground velocity structures and mechanical properties has been in real progress and has found various applications in the field of waste disposal (Lanz et al., 1998), landslides (Grandjean et al., 2007), or hydrogeophysics (Sturtevant et al., 2004). New equipments with 48 or 72 channels and PC-piloted acquisition software contributed to the development of this method, for example by reducing the acquisition times with unplugged gambled

sensors (Grandjean, 2006a). This improvement was also supported by the development of new data processing protocols like acoustical tomography (Azaria et al., 2003; Grandjean, 2006b) or Spectral Analysis of Surface Waves (Park et al., 2000; Grandjean and Bitri, 2006) and its multichannel application MASW (Foti, 2000; Miller, 1999). The adaptation of seismic methods to soil properties mapping is conditioned by the possibility to reduce the seismic antenna (originally of several tens of meters) to around several meters, in order to investigate the first two meters of the ground. This implies to work with very high source frequencies for dealing with high resolution data. We propose to use a small hammer to generate signals in the 1 KHz frequency range and sensors with a 100 Hz main frequency.

2.7.3. Strengths and limitations

The main problem of seismic technique is that properties deducted from this kind of geophysical data will be identified through significant research investment. Using seismic techniques we expect to produce at the catchment scale the distribution of seismic velocities (P and S-waves) along cross sections reaching 1 or 2 m depth. As the resolution is depending on the frequencies available in the recorded signal we expect to have several cm of resolution in order to identify the soil layering and at least the depth of the bedrock, both are important parameters to characterize erosion and compaction processes. Following this way of thinking, the main expected progress will be to adapt the seismic source and the seismic antenna for working at high frequencies with the capability to be moved quickly; In this way, The eventuality of sensors coupled and united to a guide for faster installation is envisaged. Besides, extraneous factor like presence of unconsolidated layers (peats, humus etc.) at the surface can affect the measurements by limiting in this case the transmission of high frequencies and in the same way the resolution. An evident advantage of the method lies in the character of properties deducted from the seismic survey which produces the only mechanical waves of the DIGISOIL project. Several other key characteristics of surface waves and surface-wave imaging give strengths to this application. First and probably foremost is the ease with which surface waves can be generated. The relative high-amplitude nature of surface waves (in comparison to body waves) makes their application in areas with elevated levels of mechanical/acoustic noise possible. A half-space is all that is necessary to propagate surface waves. Surface-wave propagation does not require the velocity to increase with depth and/or a contrast at a boundary (i.e., velocity, density, or combination [acoustic impedance]). Conductivity of soils, electrical noise, conductive structures, and buried utilities all represent significant challenges to electrical or EM methods. These have little or no impact on the generation or propagation and generally no influence on the processing or interpretation of surface-wave data. This flexibility in acquisition and insensitivity to environmental noise allow successful use of shear-wave velocity profiling in areas where other geophysical methods may be limited.

2.7.4. Available commercial sensors

Key features of commonly used seismic instruments are presented in *Table 10*. A more detailed sheet of comparison can be found in Appendix B. There is a wide variety of

commercial and non-commercial seismic instruments available, which are used in oil prospecting, that are not included. The ones listed here in *Table 10* and in Appendix B are instruments generally used in environmental and engineering surveys. Additional channels refers to if the number of available channels can be expanded by linking together two or more units.

Instrument		# of Channels	Additional channels	Sampling rate (µs)	Frequency range
Mark	**Model**				
ABEM	**Terraloc Mk8**	4-24 (in steps of 4) 4-48 (in steps of 4)	☑	25, 50, 100, 200, 500, 1000, 2000	1 - 4000 Hz
Geometrics	**SmartSeis SE**	12, 24	**No info**	31, 64, 125, 250, 500, 1000, 2000	
	StrataVisor NZ XP	3 to 64 (contr for Geode)	☑	20, 31, 62, 125, 250, 500, 1000, 2000, 4000, 8000, 16000	1,75 - 20000 Hz
	Geode	3, 6, 8, 12, 16, 24	☑	20, 3, 62, 125, 250, 500, 1000, 2000, 4000, 8000, 16000	1.75 - 20000 Hz
	ES-3000	8, 12	**No info**	62.5, 125, 250, 500, 1000, 2000	1.75 Hz - 820 kHz
PASI	**16S24-4**	12, 24	☑	32 to 2000	
OYO	**Handy Viewer McSEIS-3**	3	**No info**	20, 50, 100, 200, 500	10 - 250 Hz 10 - 2000 Hz
	McSEIS-SX(XP)	1, 3, 6, 12 or 24 +1 AUX	**No info**	33.3, 50, 100, 200, 500, 1000, 2000, 4000	2 - 4600 Hz
	McSEIS-SX48(XP)	1, 3, 6, 12, 24 or 48 +2 AUX	**No info**	33.3, 50, 100, 200, 500, 1000, 2000, 4000	2 - 4600 Hz
Seistronix	**EX-6/12**	6/12 per instrument max 3200	☑	125, 250, 500, 1000, 2000, 4000	2 - 3200 Hz
	RAS-24	12, 24 per RAS max 120 channels	☑	125, 250, 500, 1000, 2000, 4000	2 - 3300 Hz

Table 10 : List of known manufacturers for seismic instruments for environmental and engineering applications and associated specifications.

3. Adapted sensing technologies and specifications for DIGISOIL

In the following section, different geophysical systems, selected from the state of the art of chapter 2, are studied in order to propose the more adapted ones with regards to the DIGISOIL's specifications described in chapter 1.

For each of the identified methods, we describe the sensor technologies (type of sensors), the system configuration (size of sensor array, source technology) and the final tuning (system components, example of data and expected results).

3.1. GEOELECTRIC

3.1.1. Sensor and specifications

As far as geoelectric measurements are concerned, the available commercial sensors are quite satisfying. Indeed, the commercial resistivimeters deliver current in a range adapted to the measurements in subsurface prospecting, especially in soils. The resolution of the measurement of resistance -- to derive resistivity -- is correct too, insofar as most of the commercial resistivimeters can record measurement with a sensitivity of 1 omh m, sometimes even less.

On the other hand, the sensors *sensu stricto*, say the electrodes, are only usually rods that can be built very easily. They are adapted to quite all the situations encountered in the field, except the measurements of a drying soil. In the latter case, the contact point between the electrode and the soil consists in a potential initial point of development for cracks. Nevertheless, technical solutions already exist to measure the electrical resistivity without putting an electrode in the material to be investigated. They consist in contact capacitive electrodes but they are still prototypes and have never been used to analyze the cracking in soil. If needed, they will be employed in the following of the project in that context.

Despite resistivimeters and electrodes are convenient, two points must be improved for the use of electrical resistivity to characterize some soil parameters:

- the inversion techniques

- the configuration of electrodes.

We will not discuss the improvement of inversion techniques in that document because it will be analyzed in another part of the project. But we can propose some improvements for the configurations of electrodes.

3.1.2. Configuration

In the project, the geoelectric is supposed to be used in two cases:

1. at the spatial scale, to analyze the evolution of clay content, water content and bulk density on few hectares.

2. at the local scale, to analyze the evolution of water content and bulk density to discuss the development of cracking.

3.1.3. Settings

At the spatial scale, the MuCEP system, described in the paragraph 2.2.2, enables the measurements of electrical resistivity with inter-electrode spacing equal to 0.5 - 1 - and 2 m. These spacings are probably not consistent to study the evolution of the bulk density in the cultivated layer, say for soil depths from 0 to 35 cm. One decisive improvement will consist in reducing the inter-electrode spacing of this system to characterize the cultivated layer. To be consistent, these measurements must be correctly georeferenced. The resistivimeter will be coupled with a dGPS for a precise localisation of the measurements.

At the local scale, 2D arrays can be used to characterize the soil structure, and especially its evolution along a season. The improvement will consist in reducing the inter-electrode spacing so that differences of bulk density in different clods can be analyzed. Different inter-electrode spacings have been tested. The most convenient is an inter-electrode spacing equal to 10 cm: in that case, the electrodes can still be manipulated and the surface of the array is large enough so that we can analyze a Representative Elementary Volume of the cultivated layer. Nevertheless, for such a small inter-electrode spacing, the distance between the electrodes must be very precise so that the interpretation of data can give reliable results. We propose to attach the electrodes to a fixed plastic pan (see Figure 16). Different configurations of these pans constituted of 12 electrodes each enable lots of geoelectric.configurations.
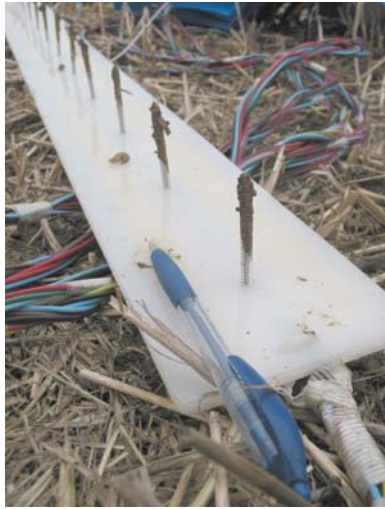
Figure 16: specific electrodes used for the characterisation of the soil structure at short scale.-a- plastic pan with electric electrodes spaced 10 cm apart. -b- Two plastic pans of 12 electrodes for a 24 Wenner array. -c- Four plastic pans of 12 electrodes for a 48 square array.

3.2. ELECTROMAGNETIC INDUCTION

As aforementioned, we intend to develop an EMI technique based on VNA technology, adapting the approach used by Lambot et al. (2004a,b) for GPR. Indeed, in contrast to existing EMI sensors, such a system would allow standard and robust calibration as well as accurate characterization of the antenna radiation properties. Moreover, full-waveform modeling of the soil response developed by the same authors could also be used, after checking for its validity for EMI.

3.2.1. Sensor and specifications

This section presents the measurements and the characterization of the EMI sensors developed in the framework of this project. However, the development of these sensors is still in progress as their sensitivity has still to be improved.

The first developed antenna consisted in a 33 cm diameter loop made of 95 turns of copper wire (section of 1.5 mm^2) connected in series with a capacitor. This antenna was connected to the first port of the VNA and was used in monostatic vertical mode. The transfer functions of the antenna (Hi: return loss transfer function; Ht: transmitting transfer function; Hr: receiving transfer function; H: product between Ht and Hr; Hf: feedback loss transfer function) were determined using the same approach as described in Lambot et al. (2004b) for GPR, i.e., measuring the ratio between the returned and the emitted signals at VNA port (S11) for several heights of the antenna over a copper sheet. Figure 17 presents the variation of the amplitude and phase of Hi, H and Hf as a function of the antenna height and frequency. The amplitudes of Hi and H vary, respectively, from minimal and maximal values at a particular frequency, which corresponds to the antenna resonant frequency (44.7 kHz in this case). This resonant frequency can be modified by adjusting the capacity of the capacitor. Minimum values of |Hi| at the resonant frequency and corresponding maximum values of |H| reveal a greater efficiency of the antenna at that frequency. Indeed, low values of |Hi| mean that large part of the emitted power is radiated while high values of |H| indicate higher transmitting and receiving performances. For the highest investigated heights, the pattern of |Hi| as a function of frequency tends quite well to that for free space conditions (i.e., at a height such that the antenna response is not influenced by the copper sheet, denominated as 'inf' in Figure 17). This result indicates that the antenna transfer functions are properly determined and that the full-waveform, three-dimensional electromagnetic model developed is adequate for our application. However, below 20 cm height, the minimal value of |Hi| shifts towards higher frequencies as the height decreases. This observation would result from near-field conditions, for which the model is not valid. Therefore, 20 cm would correspond to the minimum height of the antenna allowing correct modeling of the sub-surface response. The highest values of |H| are observed between 20 cm and 40 cm height. Moreover, |H| is rather constant within this height interval while rather strong variations are observed for higher antenna elevation, as a result of a decrease of the signal-to-noise ratio. All these observations show that model validity and antenna efficiency are acceptable between 20 and 40 cm height above the copper sheet.

This experiment allowed to attest the possibility of adapting to EMI the approach developed by Lambot et al. (2004a,b) for GPR. Nevertheless, the rather low height (40 cm) at which the efficiency of the present antenna starts to decrease sharply above the copper sheet indicates that the sensitivity of this antenna is not sufficient and that it has to be improved to be used in field conditions.

3.2.2. Configuration and settings: optimizing the current prototype system

The antenna sensitivity may potentially be improved in several ways, as listed here below:

- **_Loop parameters_**: the radiation resistance of a loop antenna being proportional to the 4th power of its **diameter**, increasing the dimension of such an antenna would be an easy way to increase its efficiency. However, for the sake of portability as well as to ensure fine spatial resolution of the measurements, the dimensions of the system should be rather limited. As a result, we do not intend to significantly increase the dimensions of the antenna beyond that of the antenna presented above (i.e., $\approx$ 33 cm diameter). Nevertheless, in the case of the 'pseudo-bistatic' mode (see below), the diameter of the receiving loop could be optimized so as to increase its efficiency while being small enough to be completely located within a so-called magnetic cavity. The radiation resistance of a loop antenna is also theoretically proportional to square of the **number of turns**. However, the number of turns, together with the **material** and the **section of the wire**, also influences the Ohmic resistance of the loop. The effects of these three parameters on antenna efficiency have already been tested and the aforementioned choices (i.e., N=95, copper wire, section=1.5 mm^2) appeared to be the optimum.

- **_Ferrite core_**: equipping the antenna with a ferrite core may allow to increase its radiation resistance and to strengthen the primary and/or the induced magnetic fields.

- **_'Pseudo-bistatic' mode_** and **_bucking coil_**: as stated above, current EMI systems are generally working in bistatic mode, i.e., separated antennas are used as transmitter and receiver. However, the approach developed by Lambot et al. (2004a,b) requests zero-offset configuration. In other respects, some EMI systems use a bucking coil so as to avoid mutual coupling between transmitter and receiver coils. The system proposed by Snow (1996) would allow to combine zero-offset bistatic mode (or 'pseudo-bistatic' mode) with the advantages provided by a bucking coil. According to this system, the transmitting antenna is made of two concentric coils: the outer coil generates the primary, strong, magnetic field while the inner coil generates a magnetic field with opposite polarity. The system is designed so that the two fields cancel exactly each other in a region centered in the two coils, creating a magnetic cavity. The receiving coil antenna, placed within the magnetic cavity, is isolated from the direct influence of the transmitting antenna and it would therefore be more sensitive to the weak magnetic field induced in the investigated sub-surface.

- **_Amplifier_**: connecting an amplifier in series between the port of the VNA and the antenna would allow to amplify the emitted signal and, as a result, to strengthen the received magnetic field.
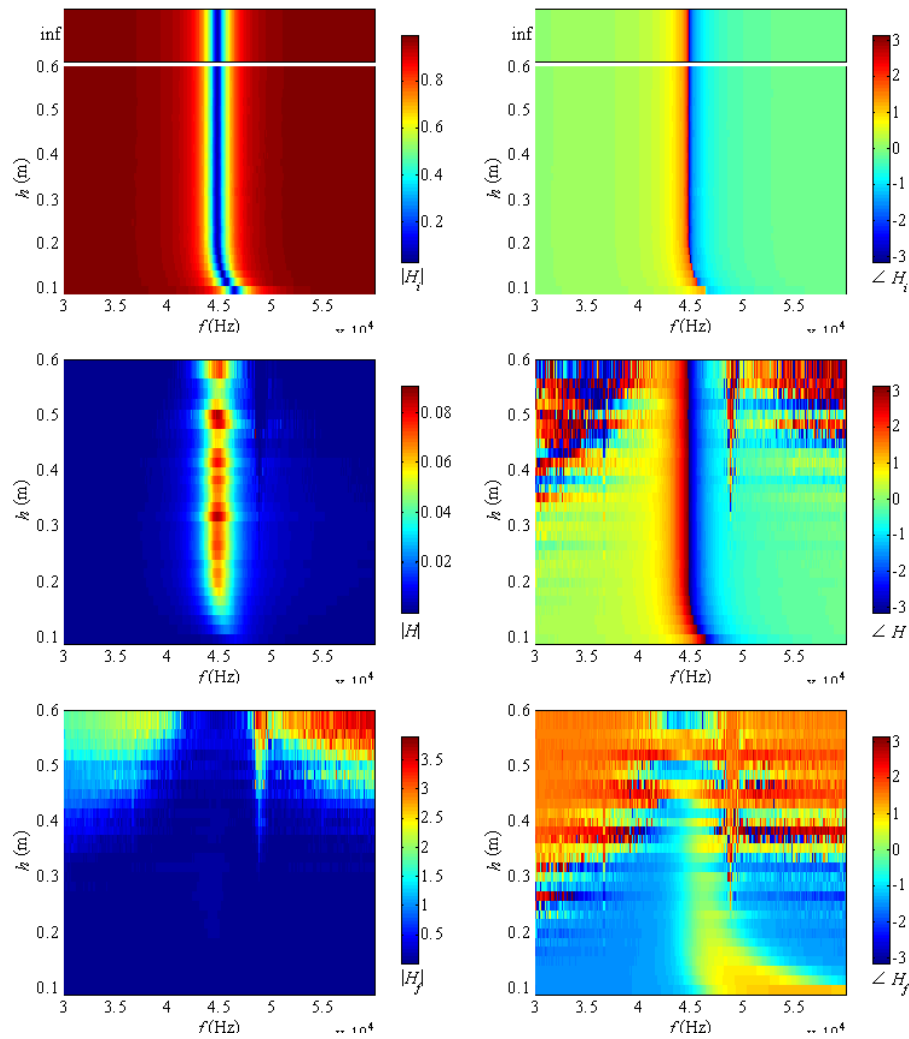
Figure 17. Amplitude and phase of the antenna transfer functions Hi, H, and Hf determined for different averaged elevations h of the antenna above a metal sheet. Measurement at 70 cm height was assumed to correspond to free-space conditions.

These factors to improve the sensitivity of the developed EMI system are being tested individually as well as in combination with each other so as to optimize the efficiency of the proposed zero-offset EMI antenna. Besides, the possibility of using simultaneously several antennas working at different frequencies as well as of combining vertical and horizontal modes will also be considered, as it would allow to get more complete information from the sub-surface.

3.3.   MAGNETISM

The definition of the optimal configuration of EMI sensors is mainly linked to the studied object. Staring form this object characteristics, theoretical simulations permit the definition of the optimal device characteristics faster and more efficiently than

experiments alone. Based on a literature review, a rapid overview of the way of choosing the geometry of the device is given in the following paragraph.

3.3.1. Sensor and geometric specifications

All the devices measuring the magnetic parameters use a coil as sensor. The main specifications of this coil are:

- its radius or side for the square-shaped ones

- the number of turns

- its position relatively to the transmitter

These three points have been discussed widely and are relatively free until the Low induction number hypothesis is valid. The existing coils perfectly filled these conditions.

There are two main classes of device geometry based on the transmitter/receiver geometry (Figure 18)

- Coincident and concentric loop configuration where transmitter and receiver are loops. The depth of investigation is of the order of magnitude of the radius.

- Slingram configuration, transmitter and receiver are small coils considered as dipole by reference to their spacing. The depth of investigation is of the order of magnitude of the spacing.
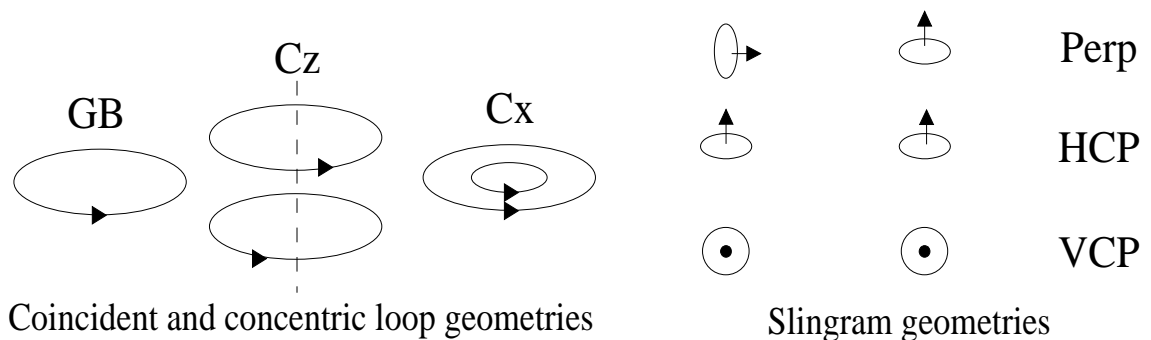
Figure 18 : Classical geometries EMI devices

The optimal configuration for studying the soil magnetic properties is the one which fits the most with the following constraints:

- A good sensitivity to the variations of the magnetic properties

- A sufficient investigation depth

Both 1D and 3D modelling are the quickest way to investigate the possibilities of a given geometry. The results shown are taken from a study looking at the κ_{qu} response but the results obtained for κ_{ph} are very similar. Some 1D modeling results are summarized on Figure 19. It shows that the 'loops' geometries are more sensitive to the upper part of the soil and slingram geometries investigate deeper.
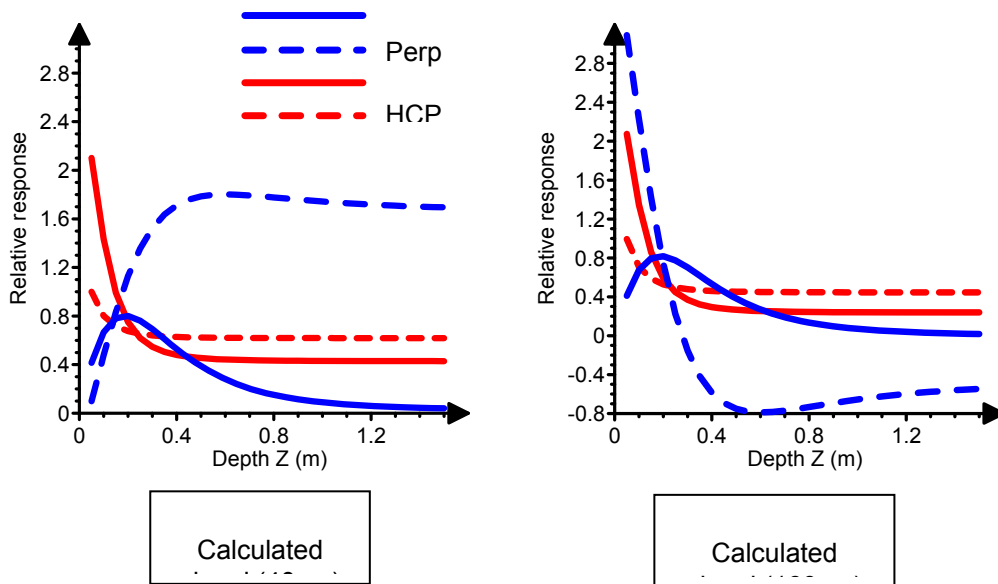
Figure 19: Some results of the 1D modeling, the 'loop' geometries appear in red and the slingram in blue

The complete studies on the subject can be read in the following papers:

- Magnetic susceptibility: Tabbagh 1986b and Benech and Marmet 1999

- Magnetic viscosity: Thiesson et al. 2007

Taking into account the mostly used geometries, it appears that the VCP (horizontal dipole) and the Perp configurations give the best results in term of magnetic properties.

3.3.2. Settings

As the measurement of magnetic properties is achieved with devices that integrate the properties over a volume, it is difficult to have several investigation depths with one device. The best choice would be multi-sensor devices, but it has to be built from nothing. To assess the interest of multi depth measurements, it would be easier, in a first step, to use two devices with geometries adapted to topsoil and subsoil. According to the 2.4.2 section, the MS2D from Bartington Ltd (Figure 20a) and MVMD from Pulsepower are well designed for topsoil measurements. The CS60 and VC100 (Figure 20b) will be used to measure the subsoil properties.

Figure 20: The choosen devices measuring the magnetic properties of soils (a) MS2D, Bartington ltd; (b) CS60 on his carriage; (c) VC100

3.4. GROUND PENETRATING RADAR

3.4.1. Sensor and specifications

Based on previous works (Lambot et al., 2008; Lambot et al., 2007; Lambot et al., 2004b; Lambot et al., 2004c; Lambot et al., 2006a; Lambot et al., 2006b; Lopera et al., 2007), the GPR system proposed within the DIGISOIL strategy is an ultra-wideband, stepped-frequency continuous-wave radar that is emulated using vector network analyzer (VNA) technology. The radar system is monostatic and operates off the ground. This particular set-up permits an accurate forward and inverse modeling of the radar signal, thereby maximizing information retrieval capabilities from the recorded data. In DIGISOIL, it is also intended to extend the capabilities of the proposed technique by improving the forward electromagnetic model so that measurements can be performed with the antenna closer to the soil for increased characterization depth and to implement antenna arrays to increase information content in the data. These two last developments will, however, probably not be completed with the DIGISOIL time frame.

The radar system can be set up using handheld VNA systems (e.g., FSH6 equipped with a VSWR bridge and power divider, Rohde&Schwarz, Munich, Germany) or any other VNA. The main advantages of the proposed technology over available commercial radar systems are:

- VNA can be simply and accurately calibrated, so that the measured quantities are fully described (calibration is an international standard). This is particularly essential when resorting to full-waveform inversion approaches for advanced and accurate signal analysis (the measured quantities are physically known and can therefore be modeled). For instance, there is no time-zero issues for such systems. Multichannel systems are also available (from 2 to 8 channels).

- It can control an ultra-wideband so that the same tool can be used with any antennas. In particular, VNA simultaneously covers both EMI and GPR frequencies (from kHz to GHz frequencies). The same VNA can then be used for simultaneous EMI and GPR measurements. An ultra-wideband is also necessary for increased resolution and information content in the data.

- It has a larger dynamic range compared to time domain systems.

- It is fully flexible, so that sensitive frequencies, which may be sensitive to state regulations, can be avoided.

The radar antenna consists of a linearly polarized, double-ridged broadband horn antenna (BBHA 9120 F, Schwarzbeck Mess-Elektronik, Schönau, Germany) operating off the ground in monostatic mode (the same antenna plays the role of both transmitter and receiver). The antenna dimensions are 96 cm high and with a 68×95 cm^2 aperture area. The antenna weight is about 16 kg. The antenna nominal frequency range is 0.2-2 GHz. The high directivity of the antenna (45° 3-dB beam width in the E- and H-planes at 1 GHz) makes it suitable for using off the ground. Measurements are performed with the antenna aperture situated at about 1.1 m above the soil surface to ensure present model adequacy (Lambot et al., 2004c). Depending on the application, different antenna types can be used. To obtain additional information from the soil, it is necessary to use antenna arrays with multiple transmitters and receivers (see above).

The antenna is connected to the reflection port of the VNA via a high quality N-type 50-Ohm coaxial cable. We calibrate the VNA at the connection between the antenna feed point and the cable using a high-quality Open-Short-Match calibration kit. The frequency-dependent complex ratio S_{11} between the returned signal and the emitted signal is measured sequentially at a series of stepped operating frequencies over the range 200-2000 MHz (usually a frequency step of 6 MHz is sufficient). Depending on the application, other frequency ranges can be used.

The system can be controlled manually, but for real-time mapping applications, it is automatically controlled with a field laptop that also records positioning data from a GPS with real-time correction (1-2 cm accuracy is reached). Figure 21 shows an example of the radar system used, in that example, for automated, real-time mapping of soil surface water content. Two different platforms where used. Figure 22 shows the obtained soil surface water content map, which is compared with a map of soil electric conductivity derived from the EM38 sensor.
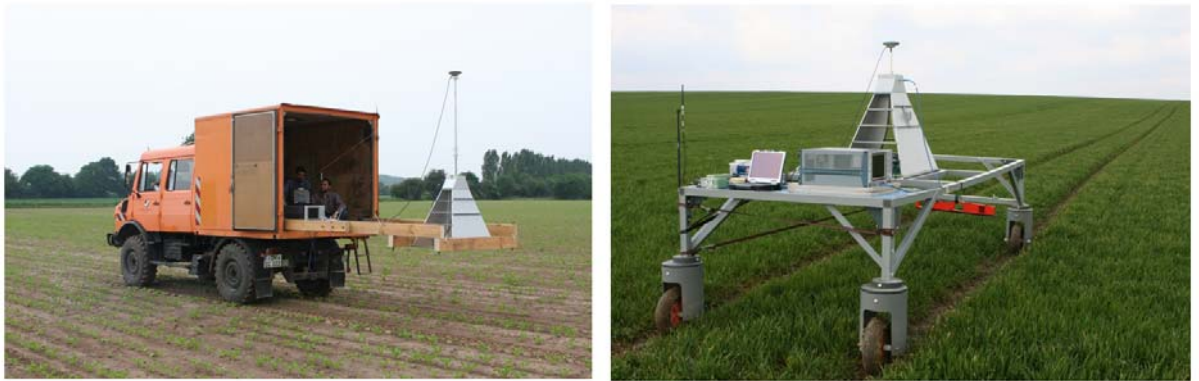
Figure 21. GPR system consisting of a vector network analyzer and a monostatic, off-ground horn antenna (200-2000 MHz) combined with a differential GPS for real-time mapping of surface soil moisture in agricultural fields. (left) Test site of the Forschungszentrum Jülich (FZJ) in Germany. (right) Test site of the Université catholique de Louvain (UCL) in Belgium. The platform in right figure is also equipped with an EMI system (EM38, Geonics) for remote soil electric conductivity determination.
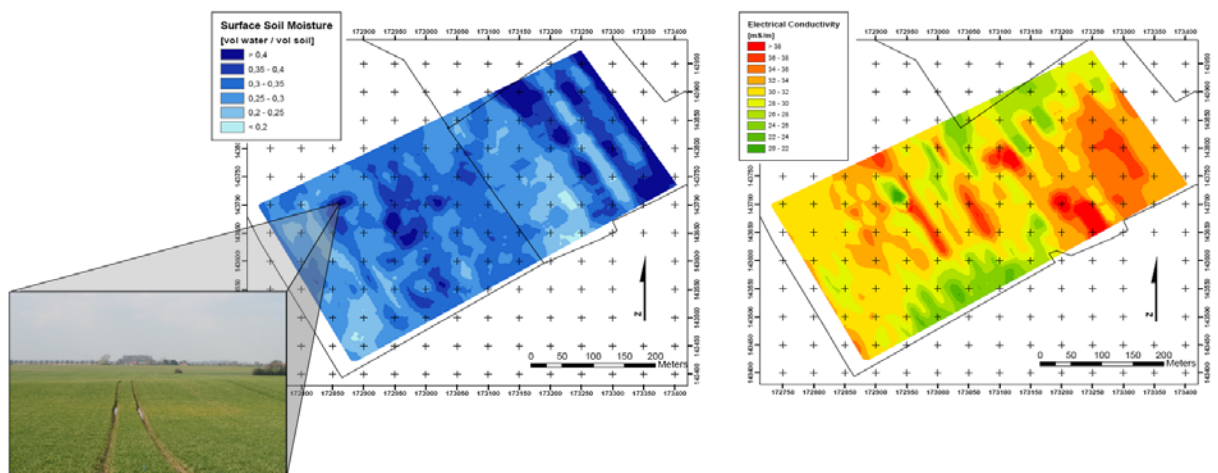
Figure 22. Surface soil moisture (left) and bulk electrical conductivity (right) in an agricultural field of 16 ha in Walhain in central Belgium. The maps were obtained from about 3000 GPR and EMI measurements using kriging. The field picture shows ponding at the soil surface, which corresponds well to a wet/saturated area in the soil moisture map.

3.5. HYPERSPECTRAL

3.5.1. Sensor and specifications

The proposed Hyperspectral System for DIGISOIL activities is the HYPER SIM.GA (Sistema Iperspettrale Multisensoriale – Galileo Avionica) is a modular avionic yperspectral system, composed mainly of two electro-optical heads in VNIR and SWIR

spectral range (from 0.4 µm to 2.5 µm) and a digital acquisition system. The first step of the development has been the realization of a "demonstrator version" tested in flight in December 2005. The system utilizes a pushbroom concept to acquire images at Nadir with a continuous spectral sampling in the VNIR-SWIR range up to over 700 channels. With reference to the available commercial sensors listed in Table 11, SIMGA is at the state of the art and comparable to the AISA DUAL system or to the coupling of CASI and SASI systems with some advantages in terms of general performance and operability (see specification tables for comparison). Moreover the SIMGA has been interested by an intensive laboratory characterization and calibration activity which can well document the intrinsic performances of sensors.

	VNIR Spectrometer	SWIR Spectrometer
Spectral Range	400-1000nm	1000 –2500nm
Spectral Sampling	1.2nm	5.8nm
Spectral bands	512	256
Spatial pixels	1024	320
IFOV	0.7mrad	1.33mrad
FOV	±19.8°]	±12°
GSD@H=1000m	0.7m	1.33m
SWATH@H=1000m	700m	425m
Focal	17 mm	22.5 mm
Digital resolution	12 bit	14 bit
Sensor	Frame transfer CCD	CMT cooled @200K
Operating Frame Rate	54Hz	27 Hz
Operating Data Rate	54MB/s	4.2MB/s
Total Data Rate	58.2MB/s	
Storage Capacity	200GB	
Max acquisition time	1h	
H/v	27s	

Table 11 : HYPER SIM.GA specifications.

3.5.2. Configuration

The modular approach allows a flexible arrangement of the instrument accommodation and therefore the possibility of its use on different platforms including ultra-light aircrafts.

The hyperspectral system is composed of the following components:
1. an optical head including the cameras; the cameras are physically separated but co-aligned on the same optical bench and enclosed in a protecting box;
2. a mechanical interface designed for different airborne
3. a rigidly mounted GPS/INS unit (inertial system) that follows the platform movements and therefore allows to storage attitude and GPS data to allow the co-registration and georeferencing of images by means of suitable tools for data post-processing;
4. a server for data acquisition and storage;

5. a power module at 28V or 220 V
6. a Tern Module for the synchronization of SIM-GA data with and attitude and GPS data
7. a Keyboard/Monitor
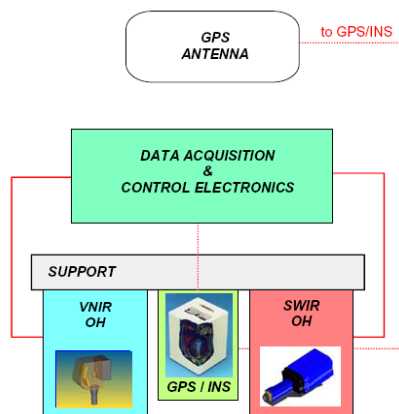
a) b)

Figure 23 : a) System block scheme; b) Prototype version.

HYPER SIM-GA was already flow both on board of two different CASA 212 planes of CGR (Parma - IT) and INTA (Madrid - ES) in 2005 and 2007, as well as on board of an Allegro 2000 ultralight plane of KELL AVIO (Rome – IT) during summer 2006 as shown in Figure 23 and Figure 24.

a) b)

Figure 24 : Installation of SIM.GA demo version on a) CASA 212 bay door; b) on Ultralight Plane Allegro 2000.

An updated SIM-GA configuration is foreseen for DIGISOIL flight activity based on the prototype version instead of demo one used for last 2007 campaigns, in order to improve system performances as well as data acquisition capabilities and operability on board of the FOLDER ultra-light plane of the Earth Science Dept. of the University of Firenze (see Figure 25).

In the Table 12 the total budget in terms of available acquisition time and total mass (SIMGA + batteries) is shown for the first DIGISOIL flight campaigns, although further improvements in terms of mass and power reductions are already foreseen for next flights.

BUDGET SIMGA		N.2 BATTERIES HESA 900			TOTAL BUDGET	
Power [W]	Mass [Kg]	Capac. [Ah]	Mass [Kg]	Energ. Disp. [KJ]	Autonomy [min.]	Mass [Kg]
535	77	26	20	1123	**60**	**97**

Table 12 : : SIM-GA power and mass budget for the ultralight plane installation.
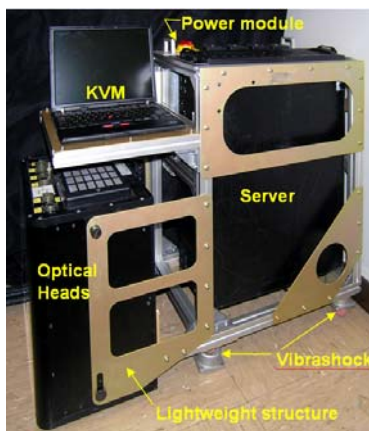
a)

b)

Figure 25 : SIMGA Configuration for DIGISOIL flights: a) lightweight instrument setup; b) the Ultralight FOLDER to be used.

3.5.3. Settings

The specific settings for the system can be described in terms of:
  a) verification of the system calibration: spectral parameters (Central Wavelength, FWHM), radiometric parameters (Flat Field, Instrument Transfer Function), geometrical parameters (IFOV, FOV, geometrical resolution across and along

track, VNIR and SWIR boresight alignement) and overall performances (SNR, NeDL, smile, keynstone). A detailed calibration report will be provided in advance of the remote sensing campaigns.

b) operational settings for in-flight data acquisition and data storage. In particular, for the radiance level at the time of the flights the optimal Integration time for VNIR and SWIR data acquisition will be evaluated in order to avoid saturation/underexposure conditions, as well as the appropriate speed and height will be selected according to the ground resolution and data rate as shown in Figure 26.
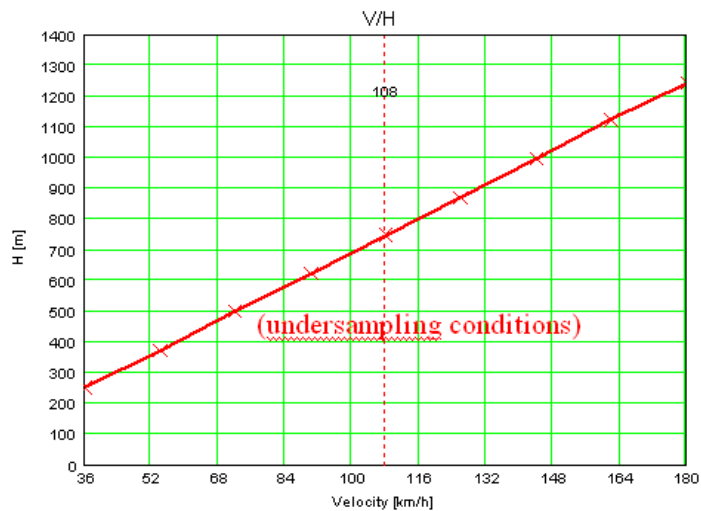
Figure 26 : V/H graph for the SIMGA configuration where for a given flight speed (e.g. 108 Km/h) the minimum flight height/speed conditions for avoiding data undersampling and blurring effect can be derived (e.g. 800m @108km/h).

c) pre-processing of raw data up to the atmospheric compensation and geocoding. The flow diagram which describes the overall procedure is shown in Figure 27.
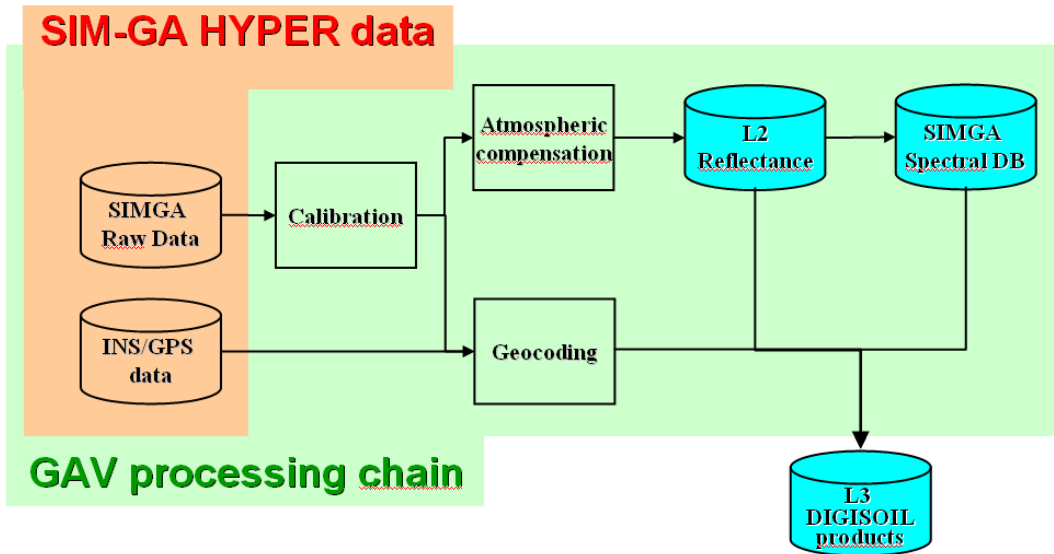
Figure 27 : Pre-processing chain for deriving hyperspectral products.

d) on-ground required measurements for atmospheric and vicarious calibration. In particular, direct solar irradiance, spectral radiance and reflectance on reference homogeneous surfaces will be measured by means of an ASD portable spectroradiometer. On that basis radiance and reflectance airborne data will be validated. (see Figure 28).

Figure 28 : Ground measurements for vicarious calibration.

3.6.   SEISMIC

The proposed seismic method is mainly based on SASW. Since the performances of SASW is closely related to the spectral response of the source and sensors used, the design of the seismic antenna – i.e., the line of sensors – we present here some tests measuring the efficiency of the method for different equipments and measuring settings. The objective is to select the best technical solutions and configurations in order to design the future acquisition system that will be used for the next field experiments.

3.6.1. Sensor and specifications: tests of seismic sources and sensors

This section presents measurements realized with different kinds of seismic sources and sensors. We focused our attention on the most relevant configuration matching the technical specifications above defined for imaging of the very shallow ground's structure with the highest resolution, this assumption implying to operate with a large frequency bandwidth. In consequence, we must gain as much as possible high frequencies in the signals, either from the impulsions generated by the source, than from the seismic data recorded by the sensors.

We have tested different seismic sources based on simple mechanical systems and providing moderate energies:

- A hammer striking on an anvil (radius about 5 cm),

- A fall of a weight (about 1 kg) and an explosive source (Figure 29).

Since the spectral content of each is not significantly different, we decided to follow our study with a hammer striking source.

For the comparison between three different types of sensors we tested:

- Geophones of 10 Hz central frequency;

- Geophones 100 Hz central frequency ;

- Gimbaled-like geophones.

A seismic antenna composed of 24 receivers spaced by 50 cm was used. According to the Figure 30 showing the amplitude spectra of recorded signals for the three cases, we can note that:

- The response of 100 Hz geophones are admittedly more spread towards high frequencies (until 200 Hz) and shows a low efficiency in the low ones. On the dispersion diagram, they only put in evidence the second and highest frequency mode of Rayleigh wave propagation.

- Gimbals are not very efficient in the high frequency band but remains sensitive in the low frequency one. The fundamental mode only is present in the dispersion diagram;

- Finally, the 10 Hz geophones offer a large coverage of the whole frequency band. The fundamental and first modes are well identified in the dispersion diagram.

From these tests, we can propose a solution based on 10 Hz geophones, staying in good agreement with the required objectives.

Figure 29: Tested seismic sources and receivers.

3.6.2. Configuration: geometry of the seismic line

The second step consisted in determining the optimum size of the seismic antenna. In particular, these tests consisted in finding the appropriate spacing between receivers to optimize the signal to noise ration and the resolution of the dispersion diagrams.

On a matter of fact, too long devices imply a loose of high frequencies due to absorption processes during the wave propagation from the source to the last geophone; on the other hand, too short devices bring difficulties to separate the different propagation modes due to a lack of resolution (poor ray parameter coverage) in the dispersion diagram.

During the tests, three receivers spacing have been used:

- 10 cm ;

- 20 cm ;

- 50 cm.

Shots points were systematically set at 50 cm from the first receiver. Figure 31 shows the dispersion diagrams for the three cases. We can deduct from this figure that the

optimal spacing that allows a precise velocity picking on the dispersion diagram is 50 cm because the maximum energy can be clearly observed on the whole bandwidth.
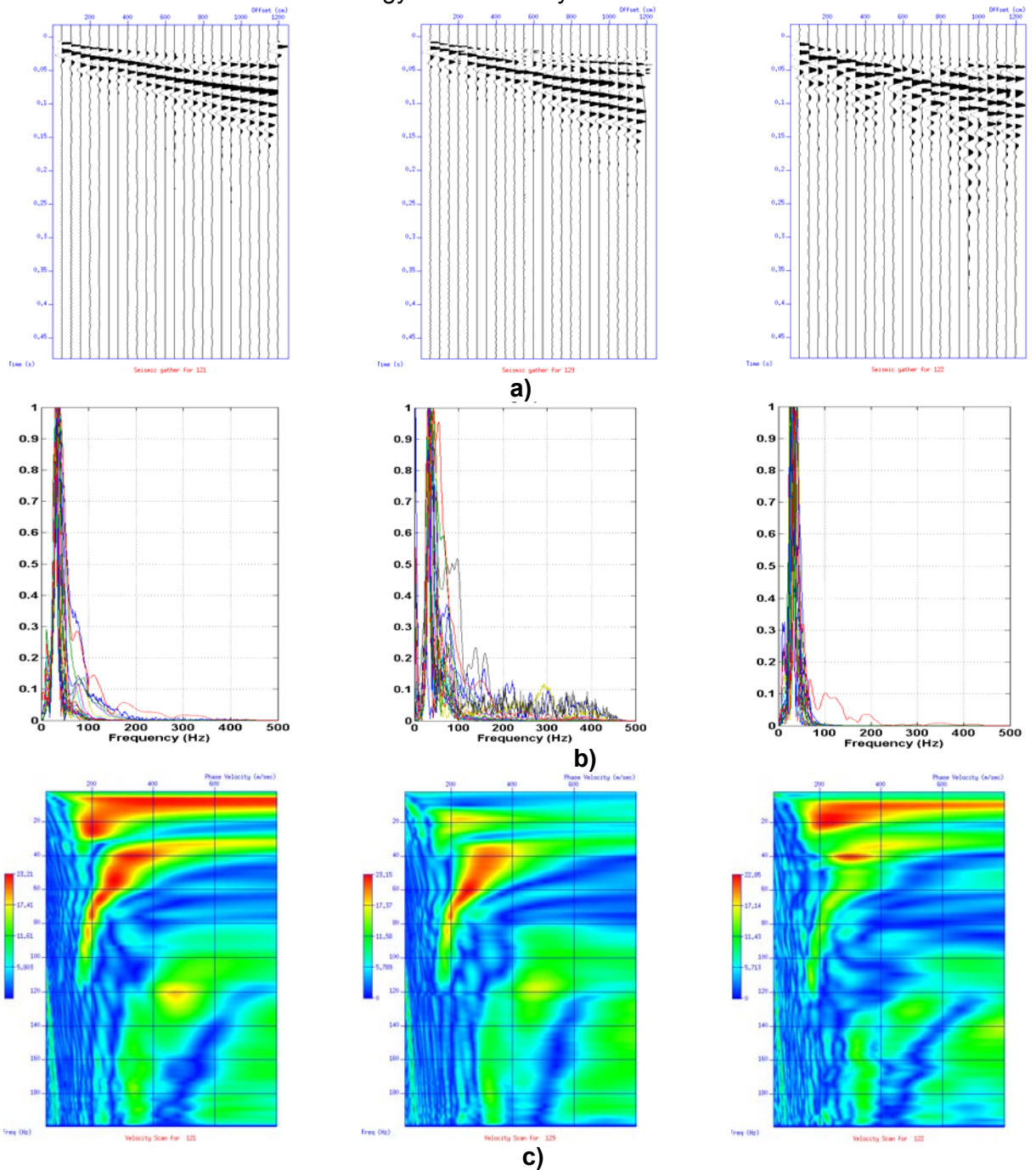
Figure 30: From left to right 10Hz, 100Hz and gimbles a) seismic gathers, b) amplitude spectra and c) dispersion diagrams.
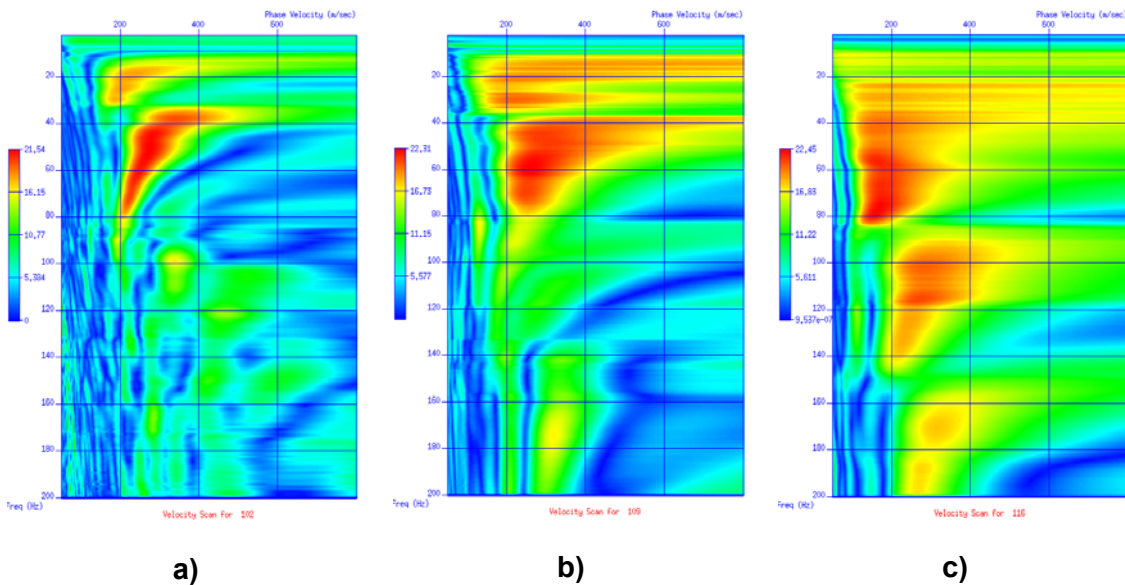
Figure 31: Dispersion diagrams for a) 50 cm spacing, b) 20 cm spacing and c) 10 cm spacing

3.6.3. Settings: final design of the seismic system

To establish the final seismic device's configuration, let's resume the acquisition system is composed by:

- A hammer striking on an anvil for generating the source signal;

- A seismic antenna of 24 receivers with central frequency of 10 Hz;

- A sensor spacing of 50 cm.

- A Geometrics GEODE unit for the numerical management of the diverse signals

- A PC-based central unit for piloting the acquisition using the Geometrics recording software;

- The optimum acquisition settings adjusted during the tests were:

  o A time recording of around 0.3-0.5 s;

  o A sampling interval of 1 ms to 250 µs;

  o No gain or filter applied on raw data;

  o No stacking before recording each shot.

The eventuality of a tractable device can be suggested to accelerate the acquisition time. The technical implementation is currently in progress, such a system being supposed to be tested during the future field experimentations. From what we can imagine, the seismic measurements would also be associated with a pseudo-automatic processing protocol coupled to a GPS tracking.

The data processing algorithms used for obtaining shear-wave velocity profiles from recorded seismic data is also being designed and will be the topic of the next deliverable of the WP1. Nevertheless, some solutions are already identified. Figure 32 shows a shear velocity profile obtained by the inversion of the dispersion curve extracted from a dispersion diagram of Figure 31. According to the associated resolution matrix – indicating on its diagonal well-constrained velocities by dark colors – this profile gives reliable shear velocity variations with depth until 10 m, let say the 7 first layers. Of course, in future works, we intend to adapt the processing protocols in order to address the specific objectives of the DIGISOIL project : erosion, compaction or shallow landslides.
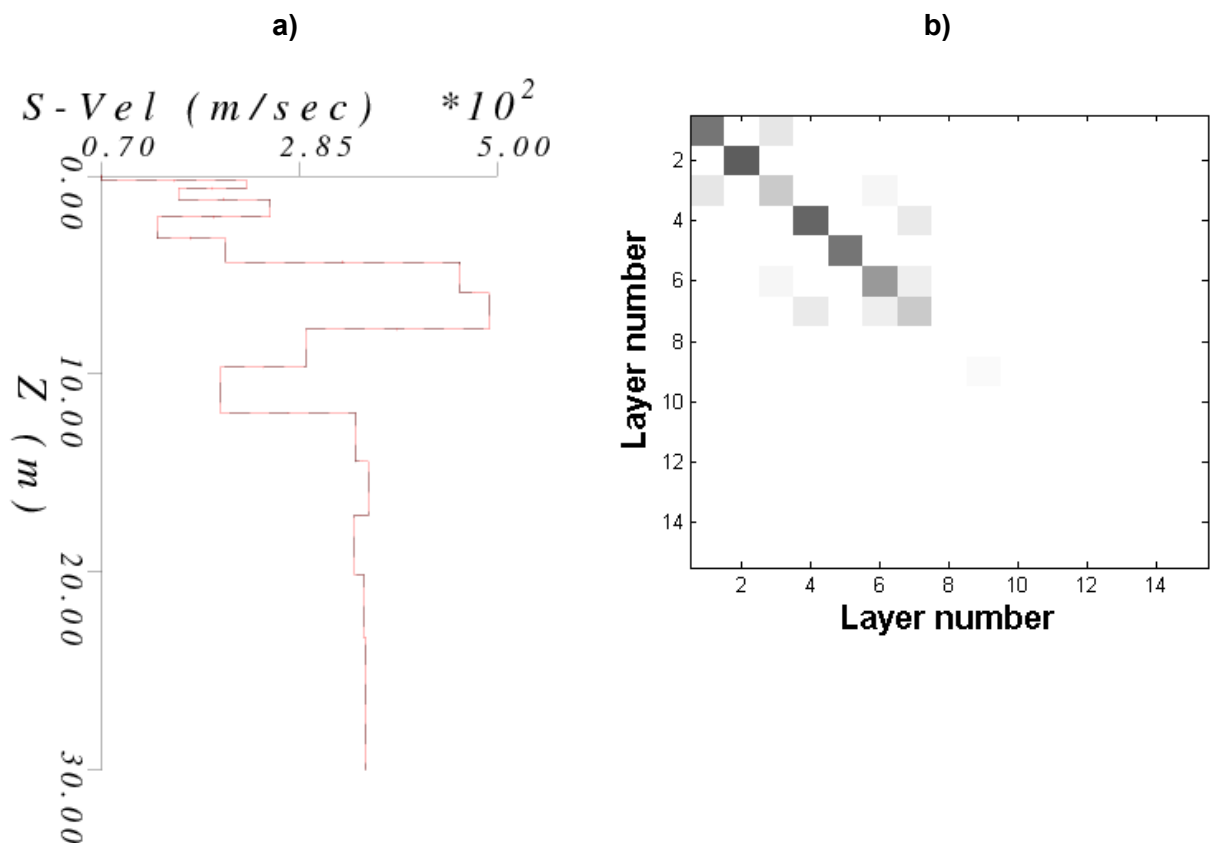
Figure 32: a) shear velocity profile obtained by inversion of Rayleigh waves dispersion curve and b) associated resolution matrix

3.7. SYNTHESIS OF THE STUDY

Techniques	Signal source	Sensors	Geometry	Piloting unit	Geolocalization	Limitations
Geoelectric (résisitivity)	DC	Electrodes	Quadripole Wienner	PC-based	Tracking GPS	High resistivity contrasts, buried pipes
EMI (resistivity)	VNA	VNA	Monostatic (array)	PC-based UCL/FZJ software	Tracking GPS piloted by the PC	EM noise
Magnetic (µ)	MVM, MS2, CS60, VC100	MVM, MS2, CS60, VC100	"Loop" (topsoil), Slingram (subsoil)	PC-based with INRA software	GPS	EM noise
GPR (dielectic constant)	VNA	VNA	Monostatic (array)	PC-based with UCL/FZJ software	Tracking GPS piloted by the PC	Too conductive shallow layers, strong soil roughness
Hyperspectral (reflectance)	Daylight	Optronics	Monostatic	GAV system	GPS	Vegetation, clouds, rain
Seismic (S-wave velocity)	Active source: 1 kg hand-driven hammer striking on a metal anvil	Geophones (10 Hz) plugged on a metal plate for moving	Linear seismic antenna composed by 24 geophones (10 Hz) and towed by a vehicle	PC-based system operating a GEODE acquisition unit with an adapted software (Geometrics)	Tracking GPS piloted by the PC.	Strong soil roughness

Table 13 : Synthesis of the study.

4. Conclusions

The present deliverable concerns the first task of the DIGISOIL's WP1. During this study, we started to analyze the requirements of the proposed system according to the data acquisition and management points of view. This part led to organize the different components of the system in the frame of a functional analysis where objectives, products and functions are clearly presented.

Then, a state of the art on the different geophysical techniques able to contribute to the Digisoil's objectives has been performed. Each technique has been reviewed in terms of measurement principles, state-of-the-art and applications, strengths and limitations, and availability of commercial and non-commercial sensors. This part led to identify the techniques being in the scope of the projects from those considered not suitable.

Finally, for all of these techniques, a study of possible technical solutions was conducted for identifying the best active source, sensors, measuring strategy and equipment. A synthetic table was proposed to roughly identify the integrated system that will be tested in the next field experiments.
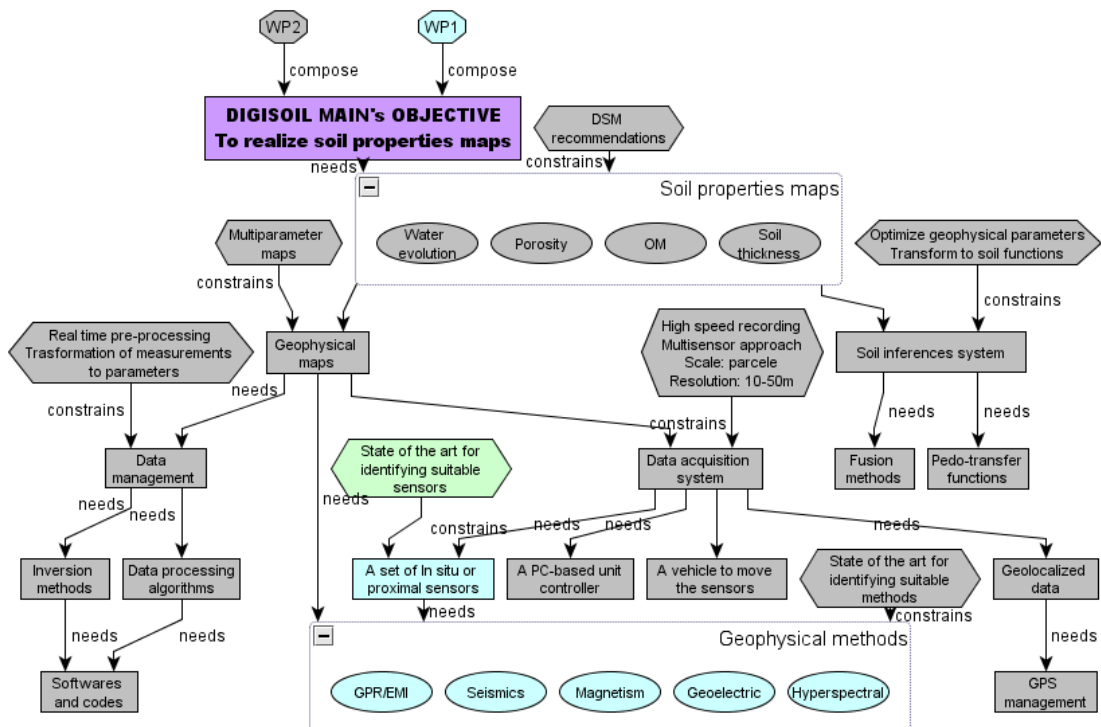
Figure 33 : components realized in the present deliverable (color) compared to those being under study (grey).

Finally, as shown in Figure 33, deliverable D1.1 contributed to the DIGISOIL's system definition by describing the geophysical methods that will be used in the next actions of the project; sensors' specifications have been identified and a first reflection on the design of measuring system has been proposed.

5. References

Aaltonen, J., 2001. Seasonal resistivity variation in some different Swedish soils. European Journal of Environmental and Engineering Geophysics, Vol. 6: 33-45.

al Hagrey, S.A. and Müller, C., 2000. GPR study of pore water content and salinity in sand. Geophysical Prospecting, 48: 63-85.

Alumbaugh, D., Chang, P., Paprocki, L., Brainard, J., Glass, R.J. and Rautman, C.A., 2002. Estimating moisture contents in the vadose zone using cross-borehole ground penetrating radar: A study of accuracy and repeatability. Water Resources Research, 38: 1309.

Anderson-Cook, C. M., and coauthors. 2002. Differentiating soil types using electromagnetic conductivity and crop yield maps. Soil Science Society of America Journal 66(5):1562-1570.

Archie G.E., 1942. The electrical resistivity log as an aid in determining some reservoir characteristics. Trans. Am. Inst. Min. Metall. Pet. Eng., 146, 54-62.

Azaria, A., C. Zelt, A. Levander, 2003. High-resolution seismic mapping at a groundwater contamination site: 3-D traveltime tomography of refraction data, EGS-AGU-EUG Joint Meeting, Nice, France.

Badea, E. A., M. E. Everett, G. A. Newman, and O. Biro. 2001. Finite-element analysis of controlled-source electromagnetic induction using Coulomb-gauged potentials. Geophysics 66(3):786-799.

Banton, O., F. Delay and G. Porel (1997). A new time domain random walk method for solute transport in 1-D heterogeneous media. Ground Water, 35(6): 1008-1013.

Benech, C.and Marmet, E. (1999). "Optimum depth of investigation and conductivity response rejection of the different electromagnetic devices measuring apparent magnetic susceptibility." *Archaeological Prospection* **6**(1): 33-45.

Bennett, D. L., and R. J. George. 1995. Using the EM38 to measure the effect of soil-salinity on Eucalyptus-globulus in south-western Australia. Agricultural Water Management 27(1):69-86.

Besson A., Cousin I., Richard G., and Boizard H., 2004. Structural heterogeneity characterization of the soil tilled layers by a 2D electrical resistivity prospecting. Soil and Tillage Research, 79, 239-249.

Binley, A., Cassiani, G., Middleton, R. and Winship, P., 2002. Vadose zone flow model parameterisation using cross-borehole radar and resistivity imaging. Journal of Hydrology, 267(3-4): 147-159.

Binley, A., Winship, P., Middleton, R., Pokar, M. and West, J., 2001. High-resolution characterization of vadose zone dynamics using cross-borehole radar. Water Resources Research, 37(11): 2639-2652.

Boll, J., van Rijn, R.P.G., Weiler, K.W., Steenhuis, T.S., Daliparthy, J. and Herbert, S.J., 1996. Using ground penetrating radar to detect layers in a sandy field soil. Geoderma, 70: 117-132.

Bongiovanni, M. V., N. Bonomo, M. de la Vega, L. Martino, and A. Osella. 2008. Rapid evaluation of multifrequency EMI data to characterize buried structures at a historical Jesuit Mission in Argentina. Journal of Applied Geophysics 64(1-2):37-46.

Borchers, B., T. Uram and J. M. H. Hendrickx, 1997. Tikhonov regularization of electrical conductivity depth profiles in field soils, Soil Science Society of America Journal 61(4): 1004-1009.

Bourennane, H., D. King, R. Le Parco, M. Isambert and A. Tabbagh, Three-dimensional analysis of soils and surface materials by electrical resistivity survey, Eur. J. Environ. Eng. Geophys. 3 (1998), pp. 5–23.

Cassiani, G. and Binley, A., 2005. Modeling unsaturated flow in a layered formation under quasi-steady state conditions using geophysical data constraints. Advances in Water Resources, 28(5): 467-477.

Cerv, V., and J. Pek. 1990. Modeling and analysis of electromagnetic-fields in 3D inhomogeneous-media. Surveys in Geophysics 11(2-3):205-229.

Chanzy, A., Tarussov, A., Judge, A. and Bonn, F., 1996. Soil water content determination using digital ground penetrating radar. Soil Science Society of America Journal, 60: 1318-1326.

Cockx, L., M. Van Meirvenne, and B. De Vos. 2007. Using the EM38DD soil sensor to delineate clay lenses in a sandy forest soil. Soil Science Society of America Journal 71:1314-1322.

Colani, C.and Aitken, M. J. (1966). "A new type of locating device II - Field trials." *Archaeometry* **9**: pp 9 - 19.

Cook, P. G. and G. R. Walker., 1992. Depth profiles of electrical-conductivity from linear-combinations of electromagnetic induction measurements, Soil Science Society of America Journal 56(4): 1015-1022.

Cook, P. G., and S. Kilty. 1992. A helicopter-borne electromagnetic survey to delineate groundwater recharge rates. Water Resources Research 28(11):2953-2961.

Cook, P. G., G. R. Walker, G. Buselli, I. Potts, and A. R. Dodds. 1992. The application of electromagnetic techniques to groundwater recharge investigations. Journal of Hydrology 130(1-4):201-229.

Corwin, D. L., and S. M. Lesch. 2005. Apparent soil electrical conductivity measurements in agriculture. Computers and Electronics in Agriculture 46(1-3):11-43.

Dahlin, T., B. Zhou, 2004. A numerical comparison of 2D resistivity imaging with 10 electrodes arrays. *Geophysical Prospecting*, 2004, 52, 379-398.

Davis, J.L. and Annan, A.P., 1989. Ground penetrating radar for high resolution mapping of soil and rock stratigraphy. Geophysical Prospecting, 37: 531-551.

Dawson, T. W., and J. T. Weaver. 1979. 3-Dimensional induction in a nonuniform thin sheet at the surface of a uniformly conducting earth. Geophysical Journal of the Royal Astronomical Society 59(3):445-462.

de Jong, E., A. K. Ballantyne, D. R. Cameron, and D. W. L. Read. 1979. Measurement of apparent electrical conductivity of soils by an electromagnetic induction probe to aid salinity surveys. Soil Science Society of America Journal 43:810-812.

Dimitriev, V. I., and N. I. Nesmeyanova. 1992. Integral equation method in three-dimensional problems of low-frequency electrodynamics. Mathematical and Computer Modelling 3:313-317.

Doolittle, J. A., K. A. Sudduth, N. R. Kitchen, and S. J. Indorante. 1994. Estimating depths to claypans using electromagnetic induction methods. Journal of Soil and Water Conservation 49(6):572-575.

Doolittle, J. A., S. J. Indorante, D. K. Potter, S. G. Hefner, and W. M. McCauley. 2002. Comparing three geophysical tools for locating sand blows in alluvial soils of southeast Missouri. Journal of Soil and Water Conservation 57(3):175-182.

Du, S. and Rummel, P., 1994. Reconnaissance studies of moisture in the subsurface with GPR. In: M.T.v.G.a.F.J.L.a.L. Wu (Editor), Proceedings of the Fifth International Conference on Ground Penetrating Radar, Waterloo cent. for Groundwater Res., Univ. of Waterloo, Waterloo, Ont., Canada, pp. 1241-1248.

Dunn, B. W., and H. G. Beecher. 2007. Using electro-magnetic induction technology to identify sampling sites for soil acidity assessment and to determine spatial variability of soil acidity in rice fields. Australian Journal of Experimental Agriculture 47(2):208-214.

Eigenberg, R. A., and J. A. Nienaber. 1998. Electromagnetic survey of cornfield with repeated manure applications. Journal of Environmental Quality 27(6):1511-1515.

Ernst, J.R., Maurer, H., Green, A.G. and Holliger, K., 2007. Full-waveform inversion of crosshole radar data based on 2-D finite-difference time-domain solutions of Maxwell's equations. IEEE Transactions on Geoscience and Remote Sensing, 45(9): 2807-2828.

Fomenko, E. Y., and T. Mogi. 2002. A new computation method for a staggered grid of 3D EM field conservative modeling. Earth Planets Space 54:499-509.

Foti, S. Multistation Methods for Geotechnical Characterization using Surface Waves, Dottorato di Ricerca in Ingegneria Geotecnica.

Freeland, R. S., J. L. Branson, J. T. Ammons, and L. L. Leonard. 2001. Surveying perched water on anthropogenic soils using non-intrusive imagery. Transactions of the Asae 44(6):1955-1963.

Friedman, S. P. 2005. Soil properties influencing apparent electrical conductivity: a review. Computers and Electronics in Agriculture 46(1-3):45-70.

Fukue, M., T. Nakamura and Y. Kato, 1999. Cementation of soils due to calcium carbonate. Soils Foundations 396 (1999), pp. 55-64.

Galagedara, L.W., Parkin, G.W. and Redman, J.D., 2003. An analysis of the GPR direct ground wave method for soil water content measurement. Hydrological Processes, 17: 3615-3628.

Galagedara, L.W., Parkin, G.W., Redman, J.D., P. and Endres, A.L., 2005a. Field studies of the GPR ground wave method for estimating soil water content during irrigation and drainage. Journal of Hydrology, 301: 182-197.

Galagedara, L.W., Redman, J.D., Parkin, G.W., Annan, A.P. and Endres, A.L., 2005b. Numerical modeling of GPR to determine the direct ground wave sampling depth. Vadose Zone Journal, 4: 1096-1106.

Garambois, S., Sénéchal, P. and Perroud, H., 2002. On the use of combined geophysical methods to assess water content and water conductivity of near-surface formations. Journal of Hydrology, 259: 32-48.

Giao, P.H., S.G. Chung, D.Y. Kim and H. Tanaka, 2003. Electrical imaging and laboratory resistivity testing for geotechnical investigation of Pusan clay deposits, Journal of Applied Geophysics 52 (2003), pp. 157-175.

Gloaguen, E., Giroux, B., Marcotte, D. and Dimitrakopoulos, R., 2007. Pseudo-full-waveform inversion of borehole GPR data using stochastic tomography. Geophysics, 72(5): J43-J51.

Grandjean G. and Bitri A., (2006) 2M-SASW: inversion of local Rayleigh wave dispersion in laterally heterogeneous subsurfaces: application to Super-Sauze landslide (France). *Near Surface Geophysics,,* 367-375.

Grandjean G., 2006b. Imaging subsurface objects by seismic P-wave tomography: numerical and experimental validations. Near Surface Geophysics, 275-283.

Grandjean, G., 2006a. A seismic multi-approach method for characterizing contaminated sites. J. Applied Geophys., 58, 87-98.

Grandjean, G., Malet, J.P., Bitri, A., and Meric O., 2007. Geophysical data fusion by fuzzy logic for imaging mechanical behaviour of mudslides. Bull. Soc. Geol. France, 177, 2, 133-143.

Grandjean, G., Paillou, P., Baghdadi, N., Heggy, E., August, T. and Lasne, Y., 2006. Surface and subsurface structural mapping using low frequency radar: A synthesis of the Mauritanian and Egyptian experiments. Journal of African Earth Sciences, 44(2): 220-228.

Grandjean, G., Paillou, P., Dubois-Fernandez, P., August-Bernex, T., Baghdadi, N.N. and Achache, J., 2001. Subsurface structures detection by combining L-band polarimetric SAR and GPR data: Example of the Pyla Dune (France). IEEE Transactions on Geoscience and Remote Sensing, 39(6): 1245-1258.

Greaves, R.J., Lesmes, D.P., Lee, J.M. and Toksov, M.N., 1996. Velocity variations and water content estimated from multi-offset, ground-penetrating radar. Geophysics, 61: 683-695.

Greenhouse, J. P., and D. D. Slaine. 1983. The use of reconnaissance electromagnetic methods to map contaminant migration. Ground Water Monitoring and Remediation 3(2):47-59.

Grote, K., Hubbard, S.S. and Rubin, Y., 2003. Field-scale estimation of volumetric water content using GPR ground wave techniques. Water Resources Research, 39(11): 1321, doi:10.1029/2003WR002045.

Hayles, J.G., M.H. Serzu, G.S. Lodha, R.A. Everitt, and D.K. Tomsons. Cross-holes seismic and signle-hole geophysical survey to characterize an area of moderately fractured granite, Canadian journal of exploration geophysics Vol 32, No. 1 (June 1996), P. 6-23.

Heller F. and. Evans M. E.. 1995. Loess magnetism. Reviews of geophysics. 33-2::211-240

Hendrickx, J. M. B., B. Baerends, Z. I. Raza, M. Sadiq, and M. Akram Chaudhry. 1992. Soil salinity assessment by electromagnetic induction of irrigated land. Soil Science Society of America Journal 56:1933-1941.

Hoekstra, P., R. Lahti, J. Hild, C. R. Bataes, and D. Phillips. 1992. Case histories of shallow time domain electromagnetics in environmental site assessment: Case history mapping migration of oil field brines from evaporation pits and ponds. Ground Water Monitoring Revue 13:110-117.

Hubbard, S., Chen, J., Williams, K., Peterson, J. and Rubin, Y., 2005. Environmental and agricultural applications of GPR. In: S.L.a.A.G. Gorriti (Editor), Proceedings of the 3rd International Workshop on Advanced Ground Penetrating Radar, Delft University of Technology, Delft, The Netherlands, pp. 45-49.

Huisman, J.A., Hubbard, S.S., Redman, J.D. and Annan, A.P., 2003. Measuring soil water content with ground penetrating radar: A review. Vadose Zone Journal, 2: 476-491.

Huisman, J.A., Snepvangers, J.J.J.C., Bouten, W. and Heuvelink, G.B.M., 2002. Mapping spatial variation in surface soil water content: comparison of ground-penetrating radar and time domain reflectometry. Journal of Hydrology, 269: 194-207.

Huisman, J.A., Sperl, C., Bouten, W. and Verstraten, J.M., 2001. Soil water content measurements at different scales: accuracy of time domain reflectometry and ground penetrating radar. Journal of Hydrology, 245: 48-58.

Jadoon, K.Z., Slob, E., Vanclooster, M., Vereecken, H. and Lambot, S., 2008. Uniqueness and stability analysis of hydrogeophysical inversion for time-lapse ground penetrating radar estimates of shallow soil hydraulic properties. Water Resources Research, (44): W09421, doi:10.1029/2007WR006639.

Job J.O., Tabbagh A. and Hachicha M.. 1995. Détermination par méthode électromagnétique de la concentration en sel d'un sol irrigué. Canadian Journal of Soil Science. .24: 75 83

Kachanoski, R. G., E. G. Gregorich, and I. J. Vanwesenbeeck. 1988. Estimating spatial variations of soil-water content using noncontacting electromagnetic inductive methods. Canadian Journal of Soil Science 68(4):715-722.

Kalinski, R.J., and Kelly, W.E. 1993. Estimating Water Contents of Soils from Electrical Resistivity,. Geotechnical Testing Journal, 16(3): 323-329

Khakural, B. R., P. C. Robert, and D. R. Hugins. 1998. Use of non-contacting electromagnetic inductive method for estimating soil moisture across a landscape. Communications in Soil Science and Plant Analysis 29(11-14):2055-2065.

Kowalsky, M.B., Finsterle, S., Peterson, J., Hubbard, S., Rubin, Y., Majer, E., Ward, A. and Gee, G., 2005. Estimation of field-scale soil hydraulic and dielectric parameters through joint inversion of GPR and hydrological data. Water Resources Research, 41: W11425, doi:10.1029/2005WR004237.

Lambot, S., Antoine, M., van den Bosch, I., Slob, E.C. and Vanclooster, M., 2004a. Electromagnetic inversion of GPR signals and subsequent hydrodynamic inversion to estimate effective vadose zone hydraulic properties. Vadose Zone Journal, 3(4): 1072-1081.

Lambot, S., E. C. Slob, I. van den Bosch, B. Stockbroeckx, and M. Vanclooster. 2004b. Modeling of ground-penetrating radar for accurate characterization of subsurface electric properties. IEEE Transactions on Geoscience and Remote Sensing 42(11): 2555-2568.

Lambot, S., Slob, E. and Vereecken, H., 2007. Fast evaluation of zero-offset Green's function for layered media with application to ground-penetrating radar. Geophysical Research Letters, 34: L21405, doi:10.1029/2007GL031459.

Lambot, S., Slob, E., Chavarro, D., Lubczynski, M. and Vereecken, H., 2008. Measuring soil surface water content in irrigated areas of southern Tunisia using full-waveform inversion of proximal GPR data. Near Surface Geophysics, 6( ): 403-410.

Lambot, S., Slob, E.C., van den Bosch, I., Stockbroeckx, B., Scheers, B. and Vanclooster, M., 2004b. Estimating soil electric properties from monostatic ground-penetrating radar signal inversion in the frequency domain. Water Resources Research, 40: W04205, doi:10.1029/2003WR002095.

Lambot, S., Slob, E.C., Vanclooster, M. and Vereecken, H., 2006a. Closed loop GPR data inversion for soil hydraulic and electric property determination. Geophysical Research Letters, 33: L21405, doi:10.1029/2006GL027906.

Lambot, S., Weihermüller, L., Huisman, J.A., Vereecken, H., Vanclooster, M. and Slob, E.C., 2006b. Analysis of air-launched ground-penetrating radar techniques to measure the soil surface water content. Water Resources Research, 42: W11403, doi:10.1029/2006WR005097.

Lanz, E., Mauer, H., Green, A.G., 1998. Refraction tomography over a buried waste disposal site. Geophysics 63, 1414– 2007-02-21.

Leblanc, A.M., R. Fortier, M. Allard, C. Cosma, S. Buteau. Seismic cone penetration test and seismic tomography in permafrost, Canadian geotechnical journal, 2004, vol. 41, n°5, pp. 796-813 [18 page(s) (article)] (1 p.3/4)

Lee, K. H., and H. F. Morrison. 1985. A numerical-solution for the electromagnetic scattering by a two-dimensional inhomogeneity. Geophysics 50(3):466-472.

Lee, K. H., D. F. Pridmore, and H. F. Morrison. 1981. A hybrid 3-dimensional electromagnetic modeling scheme. Geophysics 46(5):796-805.

Lesch, S. M., D. J. Strauss, and J. D. Rhoades. 1995a. Spatial prediction of soil-salinity using electromagnetic induction techniques .1. Statistical prediction models - a comparison of multiple linear-regression and cokriging. Water Resources Research 31(2):373-386.

Lesch, S. M., D. J. Strauss, and J. D. Rhoades. 1995b. Spatial prediction of soil-salinity using electromagnetic induction techniques .2. An efficient spatial sampling algorithm suitable for multiple linear-regression model identification and estimation. Water Resources Research 31(2):387-398.

Linde, N., Binley, A., Tryggvason, A., Pedersen, L.B. and Révil, A., 2006. Improved hydrogeophysical characterization using joint inversion of cross-hole electrical resistance and ground-penetrating radar traveltime data. Water Resources Research, 42: W12404, doi:10.1029/2006WR005131.

Liu Q., J. Torrent, B. A. Maher, Y. Yu, C. Deng R. Zhu and Zhao X.. 2005. Quantifying grain size distribution of pedogenic magnetic particles in Chinese loess and its significance for pedogenesis. J. G. R. 110. B11102

Loke, M.H., Barker R.D., 1996. Rapid least-squares inversion of apparent resistivity pseudosections using a quasi-Newton method. *Geophysical Prospecting*, 44, 131-152.

Lopera, O., Slob, E.C., Milisavljevic, N. and Lambot, S., 2007. Filtering soil surface and antenna effects from GPR data to enhance landmine detection. IEEE Transactions on Geoscience and Remote Sensing, 45(3): 707-717.

Lunt, I.A., Hubbard, S.S. and Rubin, Y., 2005. Soil moisture content estimation using ground-penetrating radar reflection data. Journal of Hydrology, 307(1-4): 254-269.

Magnin, O. Utilisation des ondes sismiques pour la caractérisation d'objets enfouis. Contribution à la mise au point d'une méthode d'imagerie sismique très haute résolution. Application à l'imagerie des fondations de pylônes du réseau de transport d'électricité, 2008

Marmet E., Bina M., Fedroff N., Tabbagh A., 1999, Relationship between human activity and the magnetic properties of soils: a case study in the medieval site of Roissy en France. Archaeological prospection 6, pp 161-170

McBride, R. A., A. M. Gordon, and S. C. Shrive. 1990. Estimating forest soil quality from terrain measurements of apparent electrical-conductivity. Soil Science Society of America Journal 54(1):290-293.

McKirdy, D. M., J. T. Weaver, and T. W. Dawson. 1985. Induction in a thin sheet of variable conductance at the surface of a stratified earth .2. 3-Dimensional theory. Geophysical Journal of the Royal Astronomical Society 80(1):177-194.

McNeill, J. D. 1980. Electromagnetic terrain conductivity measurement at low induction numbers. Geonics Limited, Technical Note TN-6, Mississauga.

McNeill, J. D. 1991. Advances in electromagnetic methods for groundwater studies. Geoexploration 27(1-2):65-80.

Michot, D., Benderitter, Y., Dorigny, A., Nicoullaud, B., King, D., Tabbagh, A., 2003. Spatial and temporal monitoring of soil water content with an irrigated corn crop cover using electrical resistivity tomography. Water Ress. Res. 39, 5, 20p.

Miller, R.D., J. Xia, C.B. Park, J.M. Ivanov. Multichannel analysis of surface waves to ma bedrock, SEG 1999.

Mitsuhata, Y. 2000. 2-D electromagnetic modeling by finite-element method with a dipole source and topography. Geophysics 65(2):465-475.

Mitsuhata, Y., T. Uchida, and H. Amano. 2002. 2.5-D inversion of frequency-domain electromagnetic data generated by a grounded-wire source. Geophysics 67(6):1753-1768.

Mullins, C. E. (1974). "The magnetic properties of the soils and their application to archaeological prospecting." *Archaeophysika* **5**: pp 143 - 347.

Nakashima, Y., Zhou, H. and Sato, M., 2001. Estimation of groundwater level by GPR in an area with multiple ambiguous reflections. Journal of Applied Geophysics, 47: 241-249.

Newman, G. A., and D. L. Alumbaugh. 1995. Frequency-domain modeling of airborne electromagnetic responses using staggered finite-differences. Geophysical Prospecting 43(8):1021-1042.

Newman, G. A., and D. L. Alumbaugh. 1997. Three-dimensional massively parallel electromagnetic inversion .1. Theory. Geophysical Journal International 128(2):345-354.

Panissod, C., 1997. Prospection électrique et électrostatique à faible profondeur à l'aide de systèmes multipôles permettant la description directe des structures en 3-D. Th. Doctorat, Université de Paris 6.

Park, C.B., Miller, R.D., Xia, J., Ivanov, J., 2000. Multichannel seismic surface-wave methods for geotechnical applications. Proc. of the First Int. Conf. on the App. of Geophys. Methodologies to Transportation Facilities and Infrastructure, St. Louis, December 11–15.

Petersen, H., Fleige, H., Rabbel, W. and Horn, R., 2005. Applicability of geophysical prospecting methods for mapping of soil compaction and variability of soil texture on farm land. Journal of Plant Nutrition and Soil Science-Zeitschrift Fur Pflanzenernahrung Und Bodenkunde, 168(1): 68-79.

Poulton, M. M., and R. A. Birken. 1998. Estimating one-dimensional models from frequency-domain electromagnetic data using modular neural networks. Ieee Transactions on Geoscience and Remote Sensing 36(2):547-555.

Redman, J.D., Davis, J.L., Galagedara, L.W. and Parkin, G.W., 2002. Field studies of GPR air launched surface reflectivity measurements of soil water content. In: L. Steven Koppenjan and Hua (Editor), Proceedings of the Ninth International Conference on Ground Penetrating Radar, Santa Barbara, California, USA, pp. SPIE 4758:156-161.

Rhoades, J.D., Raats, P.A.C. and Prather, R.J., 1976. Effects of liquid-phase electrical conductivity, water content, and surface conductivity on bulk soil electrical conductivity. Soil Science Society of America Journal, 40: 651-655.

Robain, H., Descloitres, M., Ritz, M. and Yene Atangana, Q. (1996) A multiscale electrical survey of a lateritic soil system in the rain forest of Cameroon. J. Appl. Geophys., 34(4), p. 237-253.

Rucker, D.F. and Ferré, T.P.A., 2004. Parameter estimation for soil hydraulic properties using zero-offset borehole radar: Analytical method. Soil Science Society of America Journal, 68(5): 1560-1567.

Rucker, D.F. and Ferré, T.P.A., 2005. Automated water content reconstruction of zero-offset borehole ground penetrating radar data using simulated annealing. Journal of Hydrology, 309(1-4): 1-16.

Rucker, M.L., 2000. Applying the Seismic Refraction Technique to Exploration for Transportation Facilities, in Geophysics 2000, The First International Conference on the Application of Geophysical Methodologies to Transportation Facilities and Infrastructure, St. Louis, Missouri, December 11-15, Paper 1-3.

Sasaki, Y., 2001. Full 3-D inversion of electromagnetic data on PC. Journal of Applied Geophysics, 46: 45-54.

Scott, W. R. 2007. Broadband electromagnetic induction sensor for detecting buried landmines. Igarss: 2007 Ieee International Geoscience and Remote Sensing Symposium, Vols 1-12:22-25.

Serbin, G. and Or, D., 2003. Near-surface water content measurements using horn antenna radar: methodology and overview. Vadose Zone Journal, 2: 500-510.

Serbin, G. and Or, D., 2004. Ground-penetrating radar measurement of soil water content dynamics using a suspended horn antenna. IEEE Transactions on Geoscience and Remote Sensing, 42: 1695-1705.

Sheets, K. R., and J. M. H. Hendrickx. 1995. Noninvasive soil-water content measurement using electromagnetic induction. Water Resources Research 31(10):2401-2409.

Siegrist, R. L., and D. L. Hargett. 1989. Application of surface geophysics for location of buried hazardous wastes. Waste Management & Research 7(4):325-335.

Solimene, R., Soldovieri, F., Prisco, G. and Pierri, R., 2007. Three-dimensional microwave tomography by a 2-D slice-based reconstruction algorithm. IEEE Geoscience and Remote Sensing Letters, 4(4): 556-560.

Spichak, V., and I. Popova. 2000. Artificial neural network inversion of magnetotelluric data in terms of three-dimensional earth macroparameters. Geophysical Journal International 142(1):15-26.

Stevens, R. J., C. J. Obric, and O. T. Carton. 1995. Estimating nutrient content of animal slurries using electrical-conductivity. Journal of Agricultural Science 125:233-238.

Stoyer, C. H., and R. J. Greenfield. 1976. Numerical-solutions of response of a 2-dimensional earth to an oscillating magnetic dipole source. Geophysics 41(3):519-530.

Sturtevant, K. A., Baker, G. S., Snyder, C., Kopczynski, S., 2004. Hydrogeophysical characterization of bedrock fracture orientations using azimuthal seismic refraction tomography. AGU, H23A-1122.

Tabbagh J., Samouëlian A., Cousin, I., Tabbagh A., 2007. Numerical modelling of direct current electrical resistivity for the characterisation of cracks in soils. Journal of Applied Geophysics, 62, 4, 313-323.

Tabbagh, A. (1986a). "Applications and advantages of the slingram electromagnetic method for archaeological prospecting" Geophysics 51-3 pp 576-584.

Tabbagh, A. (1986b). "What is the best coil orientation in the Slingram electromagnetic propecting method." *Archaeometry* **28**(2): pp 185 -196.

Tabbagh, A., C. Panissod, C. Benech, M. Dabas, A. Jolivet, R. Guerrin, 2002: Un outil de reconnaissance géophysique en milieu urbain: la prospection électrostatique, Revue française de Géotechnique, 101, p. 3-10.

Thiesson J., A. Tabbagh and Flageul S. 2007. TDEM magnetic viscosity prospecting using Slingram coil configuration. Near Surface Geophysics. 5-6,:363-374.

Thompson R. and Oldfield f. 1986. Environmental magnetism. London. Allen and Unwin. 276 p

Tite M. S., Mullins C., 1971, Enhancement of the magnetic susceptibility of soils on archaeological sites., Archaeometry 13(2), pp 154-166

Tsoflias, G.P., Halihan, T. and Sharp, J.M., 2001. Monitoring pumping test response in a fractured aquifer using ground-penetrating radar. Water Resources Research, 37(5): 1221-1229.

Unsworth, M. J., B. J. Travis, and A. D. Chave. 1993. Electromagnetic induction by a finite electric-dipole source over a 2-D earth. Geophysics 58(2):198-214.

van Overmeeren, R.A., Sariowan, S.V. and Gehrels, J.C., 1997. Ground penetrating radar for determining volumetric soil water content: results of comparative measurements at two test sites. Journal of Hydrology, 197: 316-338.

Vasseur, G., and P. Weidelt. 1977. Bimodal electromagnetic induction in nonuniform thin sheets with an application to northern Pyrenean induction anomaly. Geophysical Journal of the Royal Astronomical Society 51(3):669-690.

Vellidis, G., Smith, M.C., Thomas, D.L. and Asmussen, L.E., 1990. Detecting wetting front movement in a sandy soil with ground penetrating radar. Trans. ASAE, 33: 1867-1874.

Wait, J. R. 1962. A note on the electromagnetic response of a stratified earth. Geophysics 27:382-385.

Ward, S. H., and G. W. Hohmann. 1987. Electromagnetic theory for geophysical applications. Pages 131-312 in M. N. Nabighian, editor. Electromagnetic methods in applied geophysics. Soc. of Exploration Geophysicists, Tulsa, OK.

Weaver, J. T., A. K. Agarwal, and X. H. Pu. 1999. 3-D finite-difference modeling of the magnetic field in geoelectromagnetic induction. Pages 426-443 in Three-Dimension Electromagnetics, volume 7. Soc Exploration Geophysicists, Tulsa.

Weiler, K.W., Steenhuis, T.S., Boll, J. and Kung, K.J.S., 1998. Comparison of ground penetrating radar and time domain reflectometry as soil water sensors. Soil Science Society of America Journal, 62: 1237-1239.

Wilford, J. and B. Minty, 2006. The use of airborne gamma-ray imagery for mapping soils and understanding landscape processes by, in Digital Soil Mapping: An Introductory Perspective, Lagacherie, P, McBratney, A. and B. Voltz, M. Ed., Elsevier Science & Technology, 600p.

Williams, B. G., and D. Hoey. 1987. The use of electromagnetic induction to detect the spatial variability of the salt and clay contents of soils. Australian Journal of Soil Research 25(1):21-27.

Windsor, C., Capineri, L., Falorni, P., Matucci, S. and Borgioli, G., 2005. The estimation of buried pipe diameters using ground penetrating radar. Insight, 47(7): 394-399.

Wollenhaupt, N. C., J. L. Richardson, J. E. Foss, and E. C. Doll. 1986. A rapid method for estimating weighted soil-salinity from apparent soil electrical-conductivity measured with an aboveground electromagnetic induction meter. Canadian Journal of Soil Science 66(2):315-321.

Xiong, Z. 1992. EM modeling three-dimensional structures by the method of system integration using integral equations. Geophysics 57:1556-1561.

Xiong, Z. H., and A. C. Tripp. 1995. Electromagnetic scattering of large structures in layered earths using integral-equations. Radio Science 30(4):921-929.

Yamashita, Y., D. Groom, T. Inazaki, and K. Hayashi. (2002) Rapid near surface resistivity survey using the capacitively-coupled resistivity system: OhmMapper.

Yelf, R., 2004. Where is true time-zero? In: E.C.S.a.A.Y.a.J. Rhebergen (Editor), Proceedings of the Tenth International Conference on Ground Penetrating Radar, Delft University of Technology, Delft, The Netherlands, pp. 279-282.

Yoder, R.E., Freeland, R.S., Ammons, J.T. and Leonard, L.L., 2001. Mapping agricultural fields with GPR and EMI to identify offsite movement of agrochemicals. Journal of Applied Geophysics, 47: 251-259.

Zhou, C., Liu, L. and Lane, J.W., 2001. Nonlinear inversion of borehole-radar tomography data to reconstruct velocity and attenuation distribution in earth materials. Journal of Applied Geophysics, 47: 271-284.

Zhou, J., J.L. Heitman, R. Horton, T. Ren, T.E. Ochsner, L. Prunty, R.P. Ewing, and T.J. Sauer. 2006. Method for maintaining one-dimensional temperature gradients in unsaturated, closed soil cells. Soil Sci. Soc. Am. J. 0:1303-1309.

Zunoubi, M. R., J. M. Jin, K. C. Donepudi, and W. C. Chew. 1999. A spectral Lanczos decomposition method for solving 3-D low-frequency electromagnetic diffusion by the finite-element method. Ieee Transactions on Antennas and Propagation 47(2):242-248.

Technical specifications of the system of geophysical sensors

Annex A

Detailed comparison between geoelectric instruments.

Technical specifications of the system of geophysical sensors

Instrument	ABEM Terrameter LS	ABEM SAS 4000 + ES10-64	ABEM SAS 1000 + ES10-64E	IRIS Syscal Pro Switch 48/72/96	IRIS Syscal Pro Deep Marin	IRIS Syscal R2	IRIS Syscal R1 Swich 48/72	IRIS Syscal Junior Swich 48/72	IRIS Syscal Kid Swich 24
General									
Resistivity	YES	YES	YES	YES	YES	YES	YES	YES	YES
Induced Polarization	YES	YES	YES	YES	NO	YES	YES	YES	NO
Self Potential	YES	YES	YES	YES		YES	YES	YES	YES
# of channels	4 or 12	4	1	10	10	1	1	1	1
Galvanic isolated Ch.	YES	YES	YES	Possibility to have fixed voltage	NO	No	No	No	No
# IP time windows	Arbitrary user defined	10 user defined	10 user defined	20		4	4	4 user defined	N/A
Memory	>1 500 000	128MB	128MB	>21000	>21000	1022	800 or 2700	2700	1400
Temperature range (ºC)	-20 to +50 (operation)	-5 to +50 (operation) -15 to +55 (storage)	-5 to +50 (operation) -15 to +55 (storage)	-20 to +70 (operation)	-20 to +70 (operation)	-20 to +70 (operation)	-20 to +70 (operation)	-20 to +70 (operation)	-10 to +50 (operation)
Display	8.4" active TFT Colour LCD	LCD, 200 x 64 pixels. 8 lines of 40 char.	LCD, 200 x 64 pixels. 8 lines of 40 char.	LCD	LCD	LCD, 2 lines x 20 char.	LCD, 2 lines x 20 char.	LCD, 2 lines x 20 char.	LCD, 2 lines x 20 char.
GUI (User Interface)	YES	NO	NO	NO	NO	NO	NO	NO	NO
Weight [kg]	12kg	Two units, 6.5 + 5.3	Two units, 6.5 + 5.1	Switch 48: 13	10	6	9.5	7	4.1
Dimensions (mm)	390 x 210 x 320	105 x 325 x 270	105 x 325 x 270	310 x 230 x 360	310 x 230 x 360	310 x 210 x 210	310 x 310 x 210	310 x 210 x 210	230 x 180 x 170
Battery	12V, 8Ah	Not recommended	Not recommended	12V, 2x7,2Ah	12V 7,5 Ah	External only? (12V)	Internal 12V, 7Ah	Internal 12V, 7Ah	Internal 12V, 6,5Ah
External power	12V DC	12V DC	12V DC	12V DC	1 to 4 12V car bat	12V DC	12V DC	12V DC	12V DC
Remote Control	YES	YES	YES	YES	YES	NO	NO	NO	NO
Enclosure IP Rating	IP66	IP66	IP66	Weather proof	Weather proof	Water resistant	Weather proof	Weather proof	Field proof
Communication	USB and Ethernet	RS232	RS232	RS232	NO	NO	NO	NO	NO
GPS	Built-in or Ext. via USB	NO	NO	Via serial port	Via serial port	NO	NO	NO	NO
Marin Application Tow array	YES	NO	NO	YES	Marin, reading every 2 sec	NO	NO	NO	NO
Marin Application fixed array	YES	YES	YES	YES	YES	YES	YES	YES	YES
Transmitter									
Output power (W)	250W	100	100	Batt+Sw.Box:250W Ext.Gen, No Sw.Box:1200 W	2000W	250wBat/1200Gen	200	100	25
Output current [mA]	Max 2500	1 - 1000	1 - 1000	Max 2500	40000	2500	2500	Max 1200	Max 500
Constant Current	YES	YES	YES	NO	NO	NO	NO	NO	NO
Output current accuracy	<0.4%	Better than 0.5 % at 100 mA	Better than 0.5 % at 100 mA	not specified	not specified	standard 0,3 % - max. 1%	standard 0,3 % - max. 1%	not specified	not specified
Max output voltage	± 600 V	± 400 V	± 400 V	± 800/1000 V	56V	± 800 V	± 600 V	± 400 V	± 200 V
Cycle time resistivity (sec)	user defined	1,4 - 56,6	1,4 - 56,6	0.2, 0.25, 0.5, 1, 2, 4, 8	150mS to 8S	0.25 - 10s	0.25, 0.5, 1 or 2s	0,5,1,2S or 0,25 to 10s	1 or 2s
Cycle time IP (sec)	user defined	up to 8	up to 8	0.2, 0.25, 0.5, 1, 2, 4, 8	not specified	0.25 - 10s	0.25, 0.5, 1 or 2s	1, 2, 4 or 8 s	N/A
Instant polarity change	YES	NO	NO	NO	NO	NO	NO	NO	N/A
Receiver									
Input voltage range	± 2.5V, ± 15V and ± 600V	± 400 V	± 400 V	± 15 V ch 1, max sum ch 2-10 15 V	± 15 V ch 1, max sum ch 2-10 15 V	± 10 V	± 10 V	± 5 V	± 2.5 V
Input impedance	>100MΩ(2.5V), 30MΩ(15V) or 20MΩ(600V)	10 MΩ	10 MΩ	100 MΩ	100 MΩ	10 MΩ	>10 MΩ	>10 MΩ	22 MΩ
A/D-conversion	24 bit	Bitstream	Bitstream	not specified	not specified	not specified	not specified	not specified	not specified
Accuracy resistivity	0.2 % typical	0.01	0.01	0.2 % typical	0.2 % typical	0.3 % typical	0.3 % typical	0.5 % typical	1 % typical
Dynamic range	>124dB	up to 140dB + 64dB automatic gain	up to 140dB + 64dB automatic gain	not specified	not specified	not specified	not specified	not specified	not specified
Resolution (theor)	3nV at 1s integr.	30 nV	30 nV	1mV	1mV	1mV	1mV	not specified	not specified
Noise Supression	SP, Power Line Freq., Digital signal processing	SP, Power Line Freq., Noise Drift Removal	SP, Power Line Freq., Noise Drift Removal	SP, Power Line Freq.	SP(?), Power Line Freq.	SP, Power Line Freq.	SP, Power Line Freq.	SP, Power Line Freq.	SP, Power Line Freq.
Full waveform storage	YES	NO	NO	NO	NO	NO	NO	NO	NO
Multi electrode									
Multi-electrode type	Built-in relay switch. External swich box(es) for large layouts	External Relay switch	External Relay switch	Build-in relay switch. External swich box for 3D	Built in Relay Swich Graphite Electrodes	N/A (Multinod sytem 16 electrodes)	Build-in relay box	Build-in relay box	Built-in relay box
Typical imaging layout	4x21, 4x16 or 2x32	4x21 electrodes (or user defined)	4x21 electrodes (or user defined)	48 ch.: 2x24, 72 ch.: 2x36, 96 ch.: 2x48	13, 2 Current and 11 for voltage	Ext. Sw.Box: 16 electrode capability + several boxes	48 channel 2x24 72 channel 2x36	48 channel 2x24 72 channel 2x36	2 x 12
Max # of electrodes	16320	256	256	4000	13, 2C, 11P	not specified	48 and 72	48 and 72	24
Take-out distance	0.5, 1, 2, 5, 10, 20, 30m or user defined	2,5,10,15,20	2,5,10,15,20	5 and 10m	4m	not specified	5 and 10m	5 and 10m	1 and 3 m
User Defined Protocols	YES	YES	YES	YES	N/A	N/A	N/A	N/A	N/A
Roll-along	4 cable system recomm. Other available	YES, 4 cables	YES, 4 cables	2 cable system	Continuously	not specified	2 cable system	2 cable system	2 cable system
Borehole logging									
Logging accessory	YES	SASLOG 300	SASLOG 300	N/A	N/A	N/A	N/A	N/A	N/A

All information is compiled from product specifications from the instrument manufacturers, generally the version available on their web-sites at the time of the compilation.

Hence the compilation is done with reservation for changes not yet documented and with reservation for future changes of specifications.

BRGM/RP- FP7-DIGISOIL-D1.1

Instrument	GF ARES	Scintrex SARIS	PASI 16gl	Allied (Campus) Tigre	AGI SuperSting R8 IP	AGI SuperSting R1 IP	AGI MiniSting + SWIFT	AGI Marin
General								
Resistivity	YES	YES	YES	YES	YES	YES	YES	YES
Induced Polarization	YES	YES	NO	NO	YES	YES	YES	YES
Self Potential	YES	YES	NO	YES	NO	YES	YES	NO
# of channels	1	1	1	1	8	1	1	8
Galvanic isolated Ch.	No	No	No	No	NO	NO	NO	NO
# IP time windows	10 adjustable	4 user defined	0	0	6 user defined	6 user defined	6 user defined	6 user defined
Memory	16mb / 70000 readings	>10 000	1500	External PC	>79000 (Res) or >26000 (RES/IP)	27300 (Res) or 16000 (RES/IP)	>3000	>30000
Temperature range (ºC)	-10 - +50	-20 to +55 (operation?)	0 - +60	Not specified	-5 to + 50	-5 to + 50	Not specified	Not specified
Display	Large LCD Display	320x240 1/4 VGA monochrome LCD	16 characters, 2 ln, backlighted LCD	80 character alphanumeric LCD	LCD, 16 lines x 30 char.	LCD, 16 lines x 30 char.	LCD, 4 lines x 20 char.	LCD, 16 lines x 30 char.
GUI (User Interface)	NO	YES	NO	NO	NO	NO	NO	NO
Weight [kg]	4.5	8.9[1] + 1.4[2]	7	6	One units, 10.2	One unit, 10.9	Two units, 6.6 + ?	One unit, 10.2
Dimensions (mm)	150 x 210 x 400	336x190x177 Sw.Box: 336x190x60	380 x 270 x 150	335 x 235 x 300	406 x 184 x 273	406 x 184 x 273	255 x 255 x 123	406 x 184 x 273
Battery	Clip-on	Clip-on	Internal 2x6V-4Ah	Internal 12V DC 7Ah	External only	External only	Build-in	External only
External power	12V DC	24V DC	Energizer	12V DC	12V or 24V DC	12V or 24V DC	12V	12V or 24V DC
Remote Control	NO	NO	NO	NO	YES	YES	NO	NO
Enclosure IP Rating	Weather proof	IP 64	Weather proof	not specified	Weatherproof keyboard	Weatherproof keyboard	Weatherproof keyboard	Water blocked cable
Communication	RS232 / USB	RS232 / USB	RS232	RS232	RS232	RS232	RS232	RS232
GPS	not specified	external (optional)	not specified	not specified	Via Serial port	not specified	not specified	Int. storage, Int. GPS?
Marin Application Tow array	NO	NO	NO	NO	YES	NO	NO	YES
Marin Application fixed array	YES	YES			YES	YES	YES	
Transmitter								
Output power (W)	300	100	450	18	200	200	Not specified	200
Output current [mA]	Max 2000	Max 1000	500	0.5 - 200	1 - 2000	1 - 2000	1 - 500	1-2000(marine), 1-1250(land)
Constant Current	NO	NO	NO	NO	NO	NO	NO	NO
Output current accuracy	not specified	± 1.25 %	not specified	not specified	not specified	not specified	not specified	not specified
Max output voltage	± 550 V	± 500 V	± 900 V	± 180 V	± 400 V	± 400 V	± 400 V	± 400 V
Cycle time resistivity (sec)	0,3 - 30s	5 or 6 Hz	0.1-9.9 s	2.1, 4.2 or 8.4 s	0,2 to 14,4	0,2 to 14,4	1.2, 3.6, 7.2 or 14.4	0.8, 3.6, 7.2 or 14.4 (marine), 1.2, 3.6, 7.2 or 14.4 (land)
Cycle time IP (sec)	max. 30s, step 20/16.66ms	1, 2, 4 or 8 s			0.5, 1, 2, 4 or 8	0.5, 1, 2, 4 or 8	1, 2, 4 or 8	1, 2, 4 or 8 (land)
Instant polarity change	NO				NO	NO	NO	NO
Receiver								
Input voltage range	± 5 V	± 40 V	± 1.28 V	± 180 V	± 10 V	± 10 V	± 500 V	± 10 V
Input impedance	20 MW	11 MW	10 MW	22 MW	>150 MΩ	>20 MΩ	>20 MΩ	>20 MΩ
A/D-conversion	not specified	not specified	16 bit floating point	not specified	not specified	not specified	not specified	not specified
Accuracy resistivity	better than 1 %	0.01	not specified	not specified	1 % in most cases	1 % in most cases	1 % in most cases	1 % in most cases
Dynamic range	>120dB	>100dB or >120dB[1]	not specified	not specified	>100dB or >120dB[1]	>100dB or >120dB[1]	>100dB or >120dB[1]	>100dB or >120dB[1]
Resolution (theor)	0.3mV	0.6mV	0.6mV	not specified	30 nV	30 nV	30 nV	30 nV
Noise Supression	SP	Power Line Freq.	Power Line Freq.	not specified	SP, Power Line Freq.	SP, Power Line Freq.	SP, Power Line Freq.	Power Line Freq.
Full waveform storage	NO	NO	NO	NO	NO	NO	NO	NO
Multi electrode								
Multi-electrode type	Smart electrodes / Switch box	Smart electrodes	N/A	Optional built-in relay switch	Smart electrodes or external relay switch	Smart electrodes or relay switch	Smart electrodes or relay switch	Smart electrodes or relay switch
Typical imaging layout	Smart electrodes: 84,96,144,192 / Sw.Box(48 takeout)	25 electrodes	N/A	32,64,128 electrodes	1 cable system or 2 cable system	1 cable system or 2 cable system	1 cable system or 2 cable system	Marine electrode cable with graphite electrodes
Max # of electrodes	200	> 65 000	N/A	32-256	28,56,84,98 or 65000	28,56,84,98 or 65000	28,56,84,98 or 65000	11
Take-out distance	not specified	not specified	N/A	1,2,5,10m	not specified	not specified	not specified	not specified
User Defined Protocols	YES	?	not specified	not specified	YES	YES	YES	not specified
Roll-along	YES	?	N/A		YES, 1 cable	YES, 1 cable	?	Tow array
Borehole logging								
Logging accessory	N/A	N/A	N/A	N/A	N/A	N/A	N/A	N/A

All information is compiled from product specifications from the instrument manufacturers, generally the version available on their web-sites at the time of the compilation.
Hence the compilation is done with reservation for changes not yet documented and with reservation for future changes of specifications.

Annex B

Detailed comparison between seismic instruments

Technical specifications of the system of geophysical sensors

	Autonomous							With PC control			
Instruments	**ABEM Terraloc Mk8**	**Geometrics SmartSeis SE**	**Geometrics StrataVisor NZ XP**	**PASI 16S24-N**	**OYO Handy Viewer McSEIS-3**	**OYO McSEIS-SX (XP)**	**OYO McSEIS-SX48 (XP)**	**Seistronix EX-6/12**	**Seistronix RAS-24**	**Geometrics Geode**	**Geometrics ES-3000**
General											
# of channels	4-24 (in steps of 4) 4-48 (in steps of 4)	12, 24	3 to 64 (contr for Geode)	12, 24	3	1, 3, 6, 12 or 24 +1 AUX	1, 3, 6, 12, 24 or 48 +2 AUX	6/12 per instrument max 3200	12, 24 per RAS max 120 channels	3, 6, 8, 12, 16, 24	8, 12
Additional channels by multiple units	Yes	No	Yes up to 1000	Yes	No			Yes	Yes	Yes	?
Sampling rate (µs)	25, 50, 100, 200, 500, 1000, 2000	31, 64, 125, 250, 500, 1000, 2000	20, 31, 62, 125, 250, 500, 1000, 2000, 4000, 8000, 16000	32 to 2000	20, 50, 100, 200, 500	33.3, 50, 100, 200, 500, 1000, 2000, 4000	33.3, 50, 100, 200, 500, 1000, 2000, 4000	125, 250, 500, 1000, 2000, 4000	125, 250, 500, 1000, 2000, 4000	20, 3, 62, 125, 250, 500, 1000, 2000, 4000, 8000, 16000	62.5, 125, 250, 500, 1000, 2000
Record lenght (ms)	3.2 to 32700	up to 24000 samples	Up to 262144 (Std) Up to 10737418 (Opt)	Up to 65536		up to 16000 samples	up to 16000 samples	0.125 to 640000	0.125 to 64000	16000 samples, optional 64000	256 - 8192
# of samples	128, 256, 512, 1024, 2048, 4096, 8192, 16384	up to 24000 samples	16000, Opt. 64000	16000, Opt. 64000		up to 16000 samples	up to 16000 samples		up to 16000 samples	16000 samples, optional 64000	4096
Delay / Pre-trig	Del: Related to sampling rate	Del: 0 - 9999 ms	Del: 0 - 100 s	Del: 0 - 16000 ms						Del: 0 - 9999 ms	Del: 0 - 9999 ms
	Pre: 0 to 100%	Pre: View not Rec.	Pre: 0 to 100%	Pre: 0 - 10 ms		Pre: 128 samples	Pre: 128 samples			Pre: 0 - 4096 samp.	Pre: 0 - 4096 samp.
Trigger inputs	Trigger coil, make/brake, geophone, TTL	make/brake, geophone	make/brake, geophone			Hammer Switch (Contact Closure), Geophone	Hammer Switch (Contact Closure), Geophone			make/brake	make/brake
A/D converter resolution	21 bit (18 + 3) Floating	20 bit (18 + 2) Floating	24 bit		8	24 bit	24 bit	24 bit	24 bit	24 bit	24 bit
Dynamic range Theoretical/measured	126 / 114 dB		144 / 105 dB					120/115dB (6ch.) 120/118dB (12ch.)	117 dB / 112 dB	144 dB / 110 dB	144 dB / 110 dB
Frequency range (Hz)	1 - 4000 Hz		1,75 - 20000 Hz		10 - 250 Hz 10 2000 Hz	2 - 4600 Hz	2 - 4600 Hz	2 - 3200 Hz	2 - 3300 Hz	1.75 Hz - 20 kHz	1.75 Hz - 820 kHz
Analog filters	12 to 240 Hz in 6 steps	No	No	Yes				?	?	Yes	Yes
Digital filters	Yes, a wide range	Yes	Yes	Yes		Yes	Yes	Yes	Yes	Yes	Yes
System											
Processor	Low power AMD LX800, 500MHz			Pentium or equivalent	N/A	ULV Intel Celeron Processor	ULV Intel Celeron Processor	In PC	In PC	In PC	In PC
Internal memory	1GB (DDR SO-DIMM)				IC RAM (JEIDA)			In PC	In PC	In PC	In PC
Hard disk space	At least 60 GB			60 GB	980 words/ channel	80 GB	80 GB	In PC	In PC	In PC	In PC
I / O port	Ethernet, 3 x USB 2.0, External VGA	RS-232, video, keyboard and printer.		USB 2.0	RS-232C	3 x USB 2.0, External Keyboard	3 x USB 2.0, External Keyboard	Ethernet + ?	Ethernet + ?		
Windows OS	Yes / XP	No	Yes, NT		No	Yes, XP	Yes, XP	In PC	In PC	In PC	In PC
Display	8,4 " Active TFT LCD, full colour, daylight visible	640x480 LCD, Visible in bright sunlight	Brilliant daylight-visible color	10.6" LCD touch screen	192 x 128 dots LCD	10.4", XGA/TFT color LCD	10.4", XGA/TFT color LCD	In PC	In PC	In PC	In PC
Instrument											
Casing	Aluminium	Plastic	Plastic	Plastic	Plastic			Aluminium	Plastic	Plastic	Plastic
Power	10 to 30 V	12 V	12 V	12 V	6 V 4xAA	12 V	12 V	12 V	12 V	12 V	12 V
Operating Temperature (ºC)	0 - 50 (24ch.) 0 - 45 (48ch.)		-5 to 35		0 - 50	0 - 45	0 - 45	-40 - 70	-30 - 70	-30 - 75	-30 - 70
Weight (kg)	16 (24ch.) 23 (48ch.)				2	8	11	2.5(6ch.)/2.7(12ch.)	4.5	3.6	3.5
Dimensions (mm)	480x260x330 (24ch.) 480x260x470 (48ch.)				110 x 222 x 77	330 x 280 x 220	330 x 280 x 260	257x163x66 (6ch.) 318x241x66 (12ch.)	267 x 343 x 152		254 x 305 x 178
Built in interpretation software	No	Yes, simple	Yes, Advanced		No	Yes	Yes	No	No	No	No
Built in plotter	No	Yes	Yes		No	No	No	No	No	No	No

All information is compiled from product specifications from the instrument manufacturers, generally the version available on their web-sites at the time of the compilation.

Hence the compilation is done with reservation for changes not yet documented and with reservation for future changes of specifications.

Scientific and Technical Centre
ARN Division
3, avenue Claude-Guillemin - BP 36009
45060 Orléans Cedex 2 – France – Tel.: +33 (0)2 38 64 34 34